Soil Dynamics and Earthquake Engineering 173 (2023) 108144

Contents lists available at ScienceDirect

Soil Dynamics and Earthquake Engineering

journal homepage: www.elsevier.com/locate/soildyn

Effects of the extended N2 method on non-linear static procedures of reinforced concrete frame structures

Cristina Cantagallo [a,*], Marco Terrenzi [a], Francesca Barbagallo [b], Mariano Di Domenico [c], Paolo Ricci [c], Guido Camata [a], Enrico Spacone [a], Edoardo Michele Marino [b], Gerardo Mario Verderame [c]

[a] Department of Engineering and Geology, University "G. D'Annunzio" of Chieti-Pescara, Viale Pindaro 42, 65127, Pescara, Italy
[b] Department of Civil Engineering and Architecture, University of Catania, via S. Sofia 64, 95125, Catania, Italy
[c] Department of Structures for Engineering and Architecture, University of Naples Federico II, Via Claudio 21, 80125, Napoli, Italy

ARTICLE INFO

Keywords:
Earthquake engineering
Nonlinear static analysis
Pushover
Nonlinear time history analysis
Fibre section model
Hysteretic section model
N2 method
Extended N2 method
Reinforced concrete structures
Structural asymmetry

ABSTRACT

This paper intends to contribute to the validation of the extended N2 nonlinear static method of seismic analysis through the study of two existing reinforced concrete frames. The scope is to further investigate the limitations of the original N2 method in predicting the seismic response of plan asymmetric buildings and to assess the higher accuracy of the extended N2 method. The two case study buildings are representative of the Italian construction between the '70s and '90s. One is designed for gravity loads only, the other is designed according to an old seismic code. Two modelling strategies are used, one with distributed and the other with lumped plastic hinges. Three eccentricities e_{CM} between centre of mass and plan geometric centre are considered (e_{CM} = 0%, 5% and 15%). The pushover analyses are carried out following the N2 method, the N2 method plus the 100:30 directional combination rule and the extended N2 method. The results are compared with those obtained from nonlinear history analyses. For each building the seismic demand is assessed for three hazard levels. The results indicate that the application of the extended N2 method significantly enhances the shape of the demand prediction, particularly for buildings with higher plan eccentricities. On the other hand, the directional combination does not significantly change the results and should be neglected.

1. Introduction

An accurate evaluation of the seismic response of buildings is a fundamental prerequisite for the safe design of new buildings and the reliable assessment of the seismic performance of existing buildings. Seismic codes provide structural engineers with a variety of methods of analysis. Linear methods of analysis are widely employed in practice because they are simple to apply, require a low computational cost, provide a compact representation of the seismic demand and structural engineers are very familiar with them after decades of use. Linear methods of analysis are effective for the design of new buildings but may be too approximate and conservative for the seismic assessment of existing buildings, whose collapse mechanisms and ductility capacity are not known *a priori*. Nonlinear methods of analysis should be recommended to determine the most critical response mechanisms of existing buildings, particularly in the case of structures that were designed for gravity loads only. There is no doubt that Nonlinear Time History Analyses (NTHAs) provide the most accurate and realistic assessment of the seismic response of a building. Nevertheless, nonlinear static (or PushOver - PO) methods are often the preferred nonlinear methods of analysis in design practice due to their simplicity, lower computational cost, and limited output data.

The original N2 method was formulated for plane frames governed by their fundamental mode of vibration [1,2]. This is often the case of low-rise buildings with both plan- and height-regularity. The Italian (D. M. 17/01/2018, Norme Tecniche per le Costruzioni 2018, NTC2018, [3]) and European (Eurocode 8, EC8, [4]) seismic codes enforce the N2 method developed by Fajfar and its co-authors in its original formulation

* Corresponding author.
E-mail addresses: cristina.cantagallo@unich.it (C. Cantagallo), marco.terrenzi@unich.it (M. Terrenzi), fbarbaga@dica.unict.it (F. Barbagallo), mariano.didomenico@unina.it (M. Di Domenico), paolo.ricci@unina.it (P. Ricci), guido.camata@unich.it (G. Camata), espacone@unich.it (E. Spacone), edoardo.marino@unict.it (E.M. Marino), verderam@unina.it (G.M. Verderame).

https://doi.org/10.1016/j.soildyn.2023.108144
Received 16 March 2023; Received in revised form 7 July 2023; Accepted 21 July 2023
Available online 28 July 2023
0267-7261/© 2023 The Authors. Published by Elsevier Ltd. This is an open access article under the CC BY license (http://creativecommons.org/licenses/by/4.0/).

[1,2]. The basic assumption is that nonlinear plane frames deform with a shape that is proportional to that of the applied static lateral forces. Strictly speaking, this assumption holds only in the linear elastic case if the frame is pushed with forces proportional to a vibration mode. The assumption may still be acceptable in the nonlinear range when the building is both plan- and height-regular and is dominated by global ductile mechanisms. For plan-irregular or asymmetric buildings the response is three-dimensional. The original N2 method underestimates the torsional effects since its formulation is based on plane frames. The present research focuses on the original N2 method and its extension to account for torsional effects, as prescribed in EC8. More advanced PO methods, such as multimodal formulations [7] and Adaptive PO methods of analysis [5,6] – that consider the contribution of the higher modes of vibration and account for changes in mode shapes due to the nonlinearities the develop in the buildings, respectively – are beyond the scope of this paper.

In the current Italian code NTC2018 [3] and in Eurocode 8 [4] the basic N2 method is enforced with at least two load patterns. NTC2018 requires a mass-proportional load pattern (that could induce soft-storey response of the building at the first level) and, if the fundamental mode of vibration in the considered load direction has a mass participation larger than 75%, a triangular or a first-mode proportional load pattern. In all cases a load pattern derived from the storey shear force distribution found from a Response Spectrum Analysis (RSA) can be used. EC8 [4] provides similar load patterns and labels them “uniform” and “modal”. Neither EC8 [4] or NTC2018 [3] indicate any limitations to the applicability of PO analyses to irregular or asymmetric structures.

Even though PO methods were originally derived for plane buildings, PO analyses are typically applied to 3D structures too by pushing the building separately in two orthogonal directions and then combing the results with the same directional combination rules used for linear methods [3,4], mainly the SRSS or the 100:30 rule. As for the effects of the torsional response of plan asymmetric structures, since the N2 method may underestimate the response of the perimeter resisting elements [10,11], EC8 [4] introduced the extended N2 method (N2ext) [8,9].

There are several publications that assess the validity of the N2 and the N2ext methods by comparing the results with those of NTHAs. However, very few works consider existing RC buildings with 3D models, possibly with axial force–bending moment interaction in the columns. In proposing the N2ext method, Fajfar et al. [8] and Kreslin and Fajfar [9] use pseudo three-dimensional structural models of a few RC and steel buildings designed for seismic loads. All buildings are represented by planar frames connected by rigid diaphragms. Each column belonging to two frames (in two directions) is modelled independently in each of the two directions. Two independent uni-axial bending rules are assigned, thus axial-bending interaction is neglected. Compatibility of the axial deformations in columns belonging to two orthogonal frames is not enforced, and it is unclear how the axial load is distributed in the above columns. The authors do not include geometric nonlinearities, though for validation analyses up to collapse the P-Delta effects should be included. Kosmopoulos and Fardis [12], Belejo and Bento [13], Oyguc et al. [14] compare the N2ext method with the NTHA but do not compare the N2ext method with the N2 method. Erduran [15] compares the performance of different pushover methods to single case studies with simple 3D configurations. Bosco et al. [16] consider a simplified single-storey building and a 8-storey RC frame building, both designed for seismic loads according to the pre standard Eurocode 8 (the same used in Ref. [9]). D’Ambrisi et al. [17] study an existing RC school using a three-dimensional fiber section model, but the ground motions are applied separately in the two building directions. Bhatt and Bento [18] analyze real existing structures, with 3D models that account for the axial force–bending moments interaction in the columns. However, they use a limited number of ground motions. The ground motion variability is reduced by increasing the number of records [19]. More specifically, the number of records has a strong contribution to the margin of error around a reference value assumed as "real response" [20]. Skoulidou and Romão [21] suggest using at least 20 ground motions. More recently, Daei and Poursha [22] compare several enhanced PO procedures, including the N2 and the N2ext methods, through the analyses plan-symmetric RC special moment-resisting frame structures with two-dimensional structural models.

In this contest, this work pursues three general objectives, mainly:

- to investigate the accuracy of the N2 method proposed by Fajfar [2] - as enforced in NTC2018 [3] - in predicting the seismic response of reinforced concrete (RC) frame buildings with different degrees of plan asymmetry;
- to evaluate the effectiveness of the extended N2 method (N2ext) proposed by Kreslin and Fajfar [9] to overcome the shortcomings of the original N2 method when applied to buildings with significant plan asymmetry. The N2ext method adjusts the plan distribution of the displacements and drift demands obtained with the N2 method by means of modification factors derived from a RSA;
- to assess the effects on the structural demand of the directional combination applied to two separate pushover analyses carried out in two different orthogonal directions (typically, the floor plan main directions) as required by some seismic codes (notably, the current Italian building code, which uses the 100:30 combination rule).

The general objectives listed above are achieved using the following approaches, some of which represent novelties with respect to previous literature works, mainly:

- the use of 3D models, with axial force–bending moment interaction in the columns;
- geometric nonlinearities in the 3D model;
- the comparison of the N2ext method with both the N2 method and the NTHA;
- the use of two existing buildings, representative of a large part of the building stock in Italy, one designed for gravity loads only and one designed according to an old, dated Italian seismic code. The buildings are doubly symmetric with respect to the stiffness distribution, but different degrees of asymmetry and torsional deformability are introduced by assigning increasing eccentricities to the floors’ centre of mass;
- the application of the study to two different structural models defined using two different approaches, one with finite-length end hinges with section fibre models that account for the N-M_x-M_y interaction in the columns, the other with zero-length end hinges with uncoupled section phenomenological laws in the two columns’ bending directions;
- the comparison between the results obtained with the N2 and N2ext methods with the NTH results obtained using different seismic hazard levels, each represented by a large set of bi-directional ground motions.

This topic is of particular interest in countries such as Italy, where most existing buildings are old and were designed for gravity loads only or according to dated seismic codes. While in some countries older buildings are demolished and rebuilt, strengthening is often preferred in Italy, thus reliable methods of analysis are fundamental to assess the building performance and identify the main structural deficiencies before and after strengthening.

Though the interest of the study is clearly international, this research was developed in the framework of the Italian research project ReLUIS-DPC 2019–2021 WP11 and stems from the need to verify the applicability of the N2ext method and its possible introduction in the revision of the current Italian Building Code.

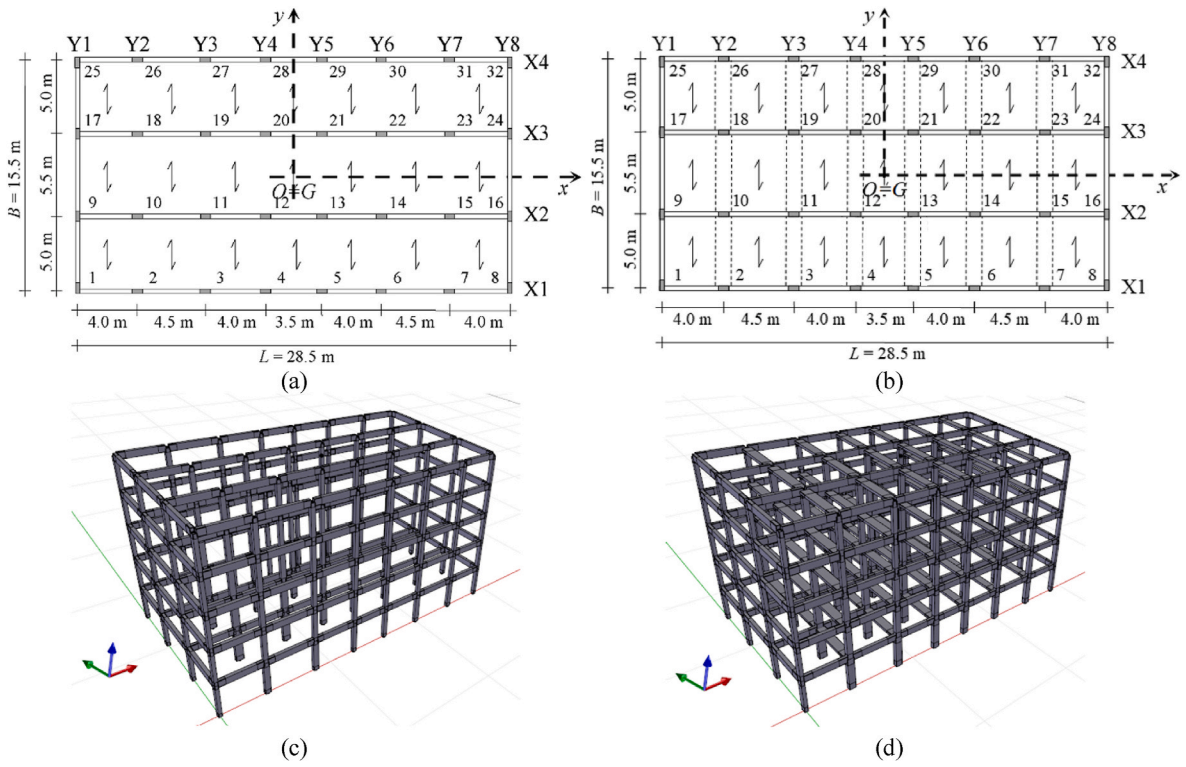

Fig. 1. Case study frames: (a) (c) plan view and 3D scheme of the Gravity Load (GL) building and (b) (d) plan view and 3D scheme of the Seismic Resistant (SR) building (the dashed lines indicate flat beams).

Table 1
Constitutive laws, schematic diagrams and values used in the structural models.

	Concrete	Non-confined concrete (GL building)	Confined concrete (SR building)	Columns
			Beams	
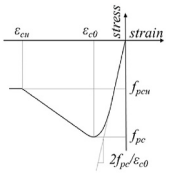	Constitutive laws	Concrete01	Concrete01	Concrete01
	Mean compressive strength	f_{pc}=28 MPa	f_{pc} = 29.55 MPa	f_{pc} = 31.58 MPa
	Strain at maximum strength	ε_{c0} = 2.5‰	ε_{c0} = 2.64‰	ε_{c0} = 2.82‰
	Strain at crushing strength	ε_{cu} = 3.5‰	ε_{cu} = 13.3‰	ε_{cu} = 21.2‰
	Crushing strength	f_{pcu}=5.6 MPa	f_{pcu}=5.91 MPa	f_{pcu}=6.32 MPa

	Steel	FeB38k (GL building)	FeB38k (SR building)
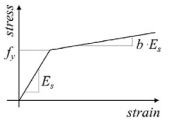	Constitutive laws	Steel01	Steel01
	Elastic Modulus	E_s = 206000 MPa	E_s = 206000 MPa
	Yield strength	f_y = 400 MPa	f_y = 450 MPa
	Strain-hardening ratio	b = 0.0049	b = 0.0049

2. Case study buildings, structural models and initial modal properties

2.1. Case study buildings

Two five-storey buildings were designed according to old Italian codes and are representative of the building stock found in towns across the seismic areas of the Mediterranean Sea. The GL building was designed to resist gravity loads only, while the SR building was designed for seismic loads. The '70s building code was used for the GL building [23] and the early '80s seismic code [24] was used for the SR building. Since most Italian RC buildings were built after World War II but before capacity design methods were enforced, the two buildings are affected by different levels of seismic deficiencies. Studying these buildings is important not only because they are designed according to old codes - thus even the SR building presents serious deficiencies with respect to current design requirements - but also because the Italian seismic zonation has considerably changed after World War II and there are areas originally classified as non-seismic that are considered today to have moderate or even high levels of seismic hazard.

The plan layout shown in Fig. 1 is rectangular and all interstorey heights are 3.2 m. The floors consist of unidirectional RC slabs - typical of Italian old constructions - made of cast-in-place RC joists separated by lightweight hollow clay bricks and topped by a 4 cm thick concrete slab. The arrows in Fig. 1 indicate the one-way slab direction. The frame arrangement provides regular distribution of stiffness and strength that is symmetric with respect to the horizontal and vertical axes passing through the plan geometric centre. Both buildings were designed following allowable stress design principles as prescribed by the two design codes used [23,25] for the GL and SR buildings, respectively.

Table 2
GL-F building: first three vibration modes after gravity load application.

Structure $e_{CM} = 0\%$				Structure $e_{CM} = 5\%$				Structure $e_{CM} = 15\%$			
T [s]	Mx	My	Rz	T [s]	Mx	My	Rz	T [s]	Mx	My	Rz
2.118	0.00%	78.72%	0.00%	2.129	0.00%	78.34%	0.41%	2.215	0.26%	75.69%	3.00%
1.227	0.00%	0.00%	80.58%	1.232	4.18%	0.37%	75.94%	1.258	22.91%	2.76%	54.41%
1.007	78.98%	0.00%	0.00%	0.998	74.79%	0.01%	4.23%	0.940	55.77%	0.20%	23.25%

Table 3
GL-H building: first three vibration modes after gravity load application.

Structure $e_{CM} = 0\%$				Structure $e_{CM} = 5\%$				Structure $e_{CM} = 15\%$			
T [s]	Mx	My	Rz	T [s]	Mx	My	Rz	T [s]	Mx	My	Rz
2.12	0.00%	81.00%	0.00%	2.14	0.00%	80.00%	1.00%	2.26	0.60%	74.34%	6.18%
1.44	0.00%	0.00%	81.89%	1.44	5.69%	1.00%	75.0 0%	1.44	23.31%	5.92%	51.68%
1.20	78.47%	0.00%	0.00%	1.19	72.76%	0.00%	5.85%	1.107	54.43%	0.70%	25.12%

Table 4
SR-F building: first three vibration modes after gravity load application.

Structure $e_{CM} = 0\%$				Structure $e_{CM} = 5\%$				Structure $e_{CM} = 15\%$			
T [s]	Mx	My	Rz	T [s]	Mx	My	Rz	T [s]	Mx	My	Rz
1.359	0.00%	76.57%	0.00%	1.370	0.01%	75.63%	0.95%	1.452	0.66%	70.23%	5.82%
0.903	0.00%	0.00%	77.34%	0.908	8.41%	0.89%	67.96%	0.927	32.91%	5.35%	38.75%
0.801	76.69%	0.00%	0.00%	0.790	68.26%	0.04%	8.44%	0.730	43.11%	0.96%	32.80%

Table 5
SR-H building: first three vibration modes after gravity load application.

Structure $e_{CM} = 0\%$				Structure $e_{CM} = 5\%$				Structure $e_{CM} = 15\%$			
T [s]	Mx	My	Rz	T [s]	Mx	My	Rz	T [s]	Mx	My	Rz
1.72	0.00%	79.12%	0.00%	1.74	0.00%	78.19%	1.00%	1.84	7.80%	72.30%	6.19%
1.29	0.00%	0.00%	79.40%	1.30	12.77%	1.00%	65.58%	1.32	37.24%	5.67%	35.86%
1.02	77.50%	0.00%	0.00%	1.03	64.92%	0.00%	13.06%	0.94	39.62%	2.00%	37.67%

Dead and live loads on structural elements are based on the nominal values given in Ref. [26].

2.1.1. Gravity load building

In the GL building the unidirectional slab is supported by four seven-bay frames parallel to the x-direction (Fig. 1a). There are two main external three-bay frames in the y direction. The beams' section is 30 × 60 cm at all floors, while the column size decreases along the height of the building. The columns' cross sections are resumed in Table A1 of the Appendix and their in-plan orientation is reported in Fig. 1a. Table A3 and Table A5 report the reinforcement details of the beams and columns, respectively.

Since most of the frames are oriented along the x-direction and almost all columns have higher stiffness and strength in the x-loading direction, the GL building has lateral stiffness and strength much larger in the x than in the y direction. This significant difference between the two horizontal directions is very common in structures designed for gravity loads only.

The concrete has compressive cubic strength $R_{ck} = 25$ MPa (corresponding to a compressive cylinder strength $f_{ck} = 20$ MPa) while steel grade Feb38K with yield stress $f_{yk} = 375$ MPa is used for reinforcement. The corresponding concrete and steel allowable stresses are 8.5 MPa and 215 MPa, respectively. The beams are modelled as continuous on multiple supports. The beams' minimum reinforcement ratio prescribed in Ref. [23] for the tension reinforcement in beams is 0.0015. The beams' shear reinforcement is designed according to the allowable stress method using 8 mm-stirrups spaced 15 cm apar in the end zones and 25 cm in the middle of the beams. Columns are designed to resist axial forces only. The bending moment is neglected according to the design practice of the '70s. The columns' design axial forces are evaluated according to the tributary area concept. Following the design code, the minimum column area $A_{c,req}$ is computed using 70% of the concrete allowable stress. The total area of the longitudinal rebars A_s in the columns is determined as the larger of $0.006\,A_{c,req}$ and $0.003\,A_c$, where A_c is the actual cross section [23]. The stirrups' spacing in the columns is designed according to the minimum provisions indicated in Ref. [23], corresponding to the minimum value between 15 times the longitudinal rebars' minimum diameter (14 mm) and 25 cm. Therefore, 8-mm diameter stirrups are used in the columns spaced 20 cm apart.

2.1.2. Old Seismic Resistant building

The plan layout of the SR building is shown in Fig. 1b. The building represents structures designed following old design provisions that simply strengthened the gravity load frames to resist the seismic lateral forces. Frames in the x-direction have deep beams, while for architectural reasons those in the y direction have flat beams, except for the external frames. The arrangement of the structural members is similar to that of the GL building thus the SR building too exhibits lateral stiffness and strength significantly larger in the x than in the direction. This situation is common to most of the buildings designed in the '80s, when the application of the seismic provisions was extended to a large part of the country, but designers were still anchored to the design for gravity loads only.

The concrete is the same of the GL building, while steel grade Feb44K reinforcement with yield stress $f_{yk} = 430$ MPa is used (steel allowable stresses = 255 MPa).

Table 6
RDRs of the GL-F building along the x- and y-directions for different values of e_{CM} and T_R.

GL-F building														
Dir.	T_R	e_{CM}	CM				Stiff Side				Flexible Side			
			N2– N2ext	N2-100:30	NTHA	1-(N2/NTHA)	N2	N2ext	N2-100:30	NTHA	1-(N2/NTHA)	N2	N2ext	N2-100:30	NTHA	1-(N2/NTHA)
x-direction	**50yr**	**5%**	0.17%	0.17%	0.13%	−26.97%	0.15%	0.20%	0.15%	0.16%	2.57%	0.18%	0.18%	0.19%	0.13%	−36.88%
		15%	0.18%	0.18%	0.12%	−44.10%	0.11%	0.23%	0.13%	0.17%	33.63%	0.21%	0.22%	0.22%	0.15%	−41.30%
	250yr	**5%**	0.38%	0.38%	0.38%	0.46%	0.34%	0.45%	0.35%	0.42%	18.29%	0.41%	0.41%	0.42%	0.39%	−6.87%
		15%	0.39%	0.40%	0.34%	−17.05%	0.26%	0.51%	0.29%	0.47%	43.91%	0.46%	0.48%	0.49%	0.39%	−19.97%
	475yr	**5%**	0.52%	0.52%	0.50%	−4.74%	0.47%	0.61%	0.48%	0.55%	14.73%	0.56%	0.56%	0.57%	0.51%	−9.45%
		15%	0.54%	0.55%	0.46%	−16.73%	0.36%	0.70%	0.40%	0.59%	39.82%	0.63%	0.66%	0.68%	0.53%	−19.00%
y-direction	**50yr**	**5%**	0.29%	0.29%	0.33%	12.07%	0.27%	0.29%	0.28%	0.30%	10.88%	0.31%	0.34%	0.32%	0.38%	17.79%
		15%	0.29%	0.30%	0.33%	10.36%	0.21%	0.29%	0.24%	0.32%	33.58%	0.34%	0.38%	0.36%	0.42%	19.31%
	250yr	**5%**	0.76%	0.76%	0.80%	4.32%	0.69%	0.76%	0.71%	0.68%	−1.07%	0.82%	0.88%	0.84%	0.94%	12.94%
		15%	0.79%	0.80%	0.76%	−4.01%	0.55%	0.79%	0.60%	0.71%	22.61%	0.92%	1.01%	0.97%	1.00%	8.27%
	475yr	**5%**	1.04%	1.05%	1.03%	−1.44%	0.95%	1.04%	0.98%	0.92%	−3.60%	1.12%	1.21%	1.14%	1.22%	8.42%
		15%	1.08%	1.10%	1.02%	−5.39%	0.75%	1.08%	0.83%	1.00%	24.57%	1.25%	1.38%	1.32%	1.28%	2.64%

Following the '80s practice, the seismic demand is found using the static lateral force method of analysis on separate plane frames. The design was carried out for two frames in each direction, one external and one internal (frames X1, X2 and Y1, Y2 in the x and y direction, respectively). All internal frames are identical and so are all external frames. The total lateral design seismic force F_h is 7% of the total seismic weight of the building [24]. The seismic design forces are distributed along the height according to an inverted triangle. Following old approaches, each frame in the x and y direction was designed to carry 1/4 and 1/8 of the total seismic load, respectively.

All deep and shallow beams have identical cross sections at all floors. The deep beam cross section is 30 × 60 cm, while the flat beam cross section is 80 × 24 cm. The column cross section sizes are reported in Table A2 of the Appendix. They depend on the column position and decrease along the building height. Table A4 and Table A6 report the reinforcement details of the beams and columns, respectively. The beams' longitudinal and shear reinforcements are designed according to the allowable stress method, considering the minimum reinforcements prescribed in Ref. [25], equal to a minimum longitudinal tension reinforcement ratio of 0.0015 and a stirrups' spacing equal to the minimum between 0.8 times the section total depth (33 cm) and, only at the beams' ends, 12 times the longitudinal rebars' minimum diameter (14 mm). For columns, the longitudinal reinforcement design considers a minimum reinforcement ratio of 0.008 and a stirrups' spacing equal to the minimum between 12 times the longitudinal rebars' minimum diameter (14 mm) and 25 cm [25]. 8 mm-diameter stirrups every 15 cm are used for all columns. For both beams and columns, the minimum requirements have strongly conditioned the design of the longitudinal and shear reinforcements.

2.2. Structural models

All models and analyses were run with the computational platform OpenSees [27] and some of the models were analysed with the pre- and post-processor STKO [28]. Two structural models were set up for each building. The first model uses *Beam-with-Hinges* elements [29] with end sections (hinges) of assigned length for all structural members. This model allows the user to specify the length of the plastic hinge whereas in other distributed plasticity models, such as the *ForceBeamColumn*, the end plastic hinges' length depends on the number of integration points. The cross sections of the finite-length end hinges are modelled using fibre sections [30], thus the effects of cracking on the element stiffness are implicitly included in the model. As for the linear elastic elements that connect the end hinges in the Beam-with-Hinges elements, their inertia is reduced to account for cracking (50% E_cI_g for beams and 80% E_cI_g for columns, where E_c is the concrete elastic modulus and I_g is the gross section inertia). These assumptions reflect the suggestion of several design codes that recommend the use of reduced elastic stiffnesses to account for section cracking. The Italian building code is generic and suggests a reduction up to 50% [3]. The ACI Code [31] suggests a lower reduction for the columns to account for the presence of the compression axial load. The end hinges' length is equal to the cross section height: for non-square columns, this length is the average of the cross section sizes. The concrete and steel fibres are modelled using the constitutive laws Concrete01 [32] and Steel01 [33], respectively. For Steel01, $E_s = 206000$ MPa, $f_y = 400/450$ MPa (for FeB38k/FeB44k steel, respectively) and strain-hardening ratio $b = 0.0049$. For non-confined concrete, $f_{pc} = 28$ MPa (corresponding to the mean concrete strength), $\varepsilon_{c0} = 2.5‰$ and $\varepsilon_{cu} = 3.5‰$ (symbols are those used in the OpenSees Manual [33]). For confined concrete, $f_{pc} = 29.55$ MPa, $\varepsilon_{c0} = 2.64‰$, $\varepsilon_{cu} = 13.3‰$ and $f_{pc} = 31.58$ MPa, $\varepsilon_{c0} = 2.82‰$, $\varepsilon_{cu} = 21.2‰$ are applied for beams and columns, respectively. For both confined and non-confined concretes, $f_{pcu} = 20\%\ f_{pc}$. Confined concrete is used for the core of cross sections of SR building only, because in the GL building the stirrup spacing is too large for an effective confinement and the stirrups have 90° rather than 135° hooks. The two structural models are labelled

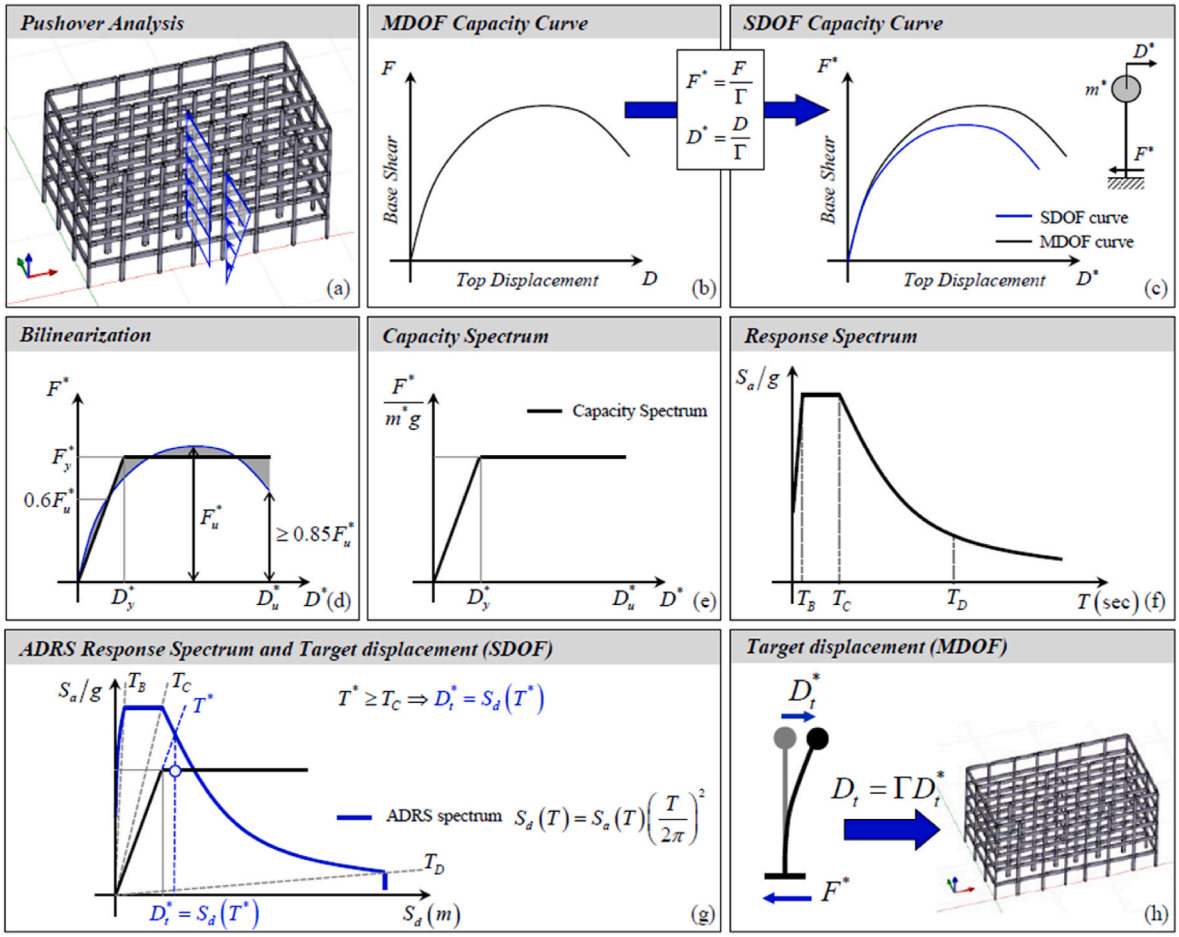

Fig. 2. N2 method schematic steps according to Ref. [3].

"GL-F" and "SR-F". Table 1 summarizes constitutive laws, schematic diagrams and values used in the structural models. All F models have floor diaphragms. The rigid diaphragm constraint prevents axial deformations in the beams of the F models, thus introducing spurious axial (generally compression) forces. To circumvent the problem, an axial buffer (zero-length) element [37] with very low axial stiffness was introduced at one end of each beam in the F models only.

The second model uses a lumped plasticity approach with two end *ZeroLength* hinges [33] connected by a linear elastic element for each structural member. The end hinges use an empirical, phenomenological macromodel with two uncoupled moment-chord rotation relationships for each plane of flexure. Unlike the fibre section model, this plastic hinge model cannot account for the M − N interaction [34]. Its behaviour requires *a priori* assumptions of the shear span (assumed equal to half the member length) and of the axial load in the columns (constant and due to gravity loads only). However, the lump plasticity model simplicity makes it very appealing, and its use is widespread in both research and design offices. The two structural models are labelled "GL-H" and "SR-H".

The phenomenological macromodel used for the *ZeroLength* hinge [33] is the model proposed by Refs. [35,36]. The Haselton material law is modelled in OpenSees with the *ModIMKPeakOriented* material [33]. It follows a tri-linear backbone curve defined by yield, peak, and zero-strength points, and cyclic strength/stiffness degradation due to cyclic energy dissipation. A set of empirical equations provide the main points of the envelope. The initial stiffness is taken as secant to 40% of the yield moment. The section yield moment was evaluated with a fibre section analysis, with the same material laws and properties used for the F models. Empirical equations were used for the peak moment, the chord rotation at peak, and the post-peak chord rotation at zero strength. Because the element flexibility is overestimated by the proposed lumped plasticity model, the stiffness correction proposed by Ref. [36] is applied. All H models have floor diaphragms.

The use of two models stems from the need to verify whether the two approaches (F and H) lead to similar trends in the application of the N2 and N2ext methods. Both F and H models neglect possible brittle failures in potentially shear-sensitive beam/column elements and/or beam-column joints. This assumption was made because the focus of the study is on the nonlinear methods of analysis rather than on capturing all the possible failure modes of the buildings. Both models include P-Delta effects.

2.3. Modal analysis

Table 2 through Table 5 report the periods and the mass participation ratios of the first three modes (computed after application of the gravity loads) of the four models GL-F, GL-H, SR-F and SR-H, respectively. Three different eccentricities e_{CM} (of CM with respect to the centre of stiffness, that coincides with the geometric centre of the plan rectangle) are considered: e_{CM} = 0%, 5% 15%. The percentage refers to the plan dimensions: e_{CM} = 5% indicates that CM is at a distance 5%L in the x positive direction and 5%B in the y positive direction with respect to the geometric centre, with L and B defined in Fig. 1. Given the plan double symmetry, any of the four possible positions corresponding to 5% and 15% eccentricities yield the same results. e_{CM} = 0% is the starting reference position, e_{CM} = 5% corresponds to the accidental eccentricity prescribed by some design codes (NTC2018 [3] and EC8 [4]) and e_{CM} =15% corresponds to a large eccentricity and represents a

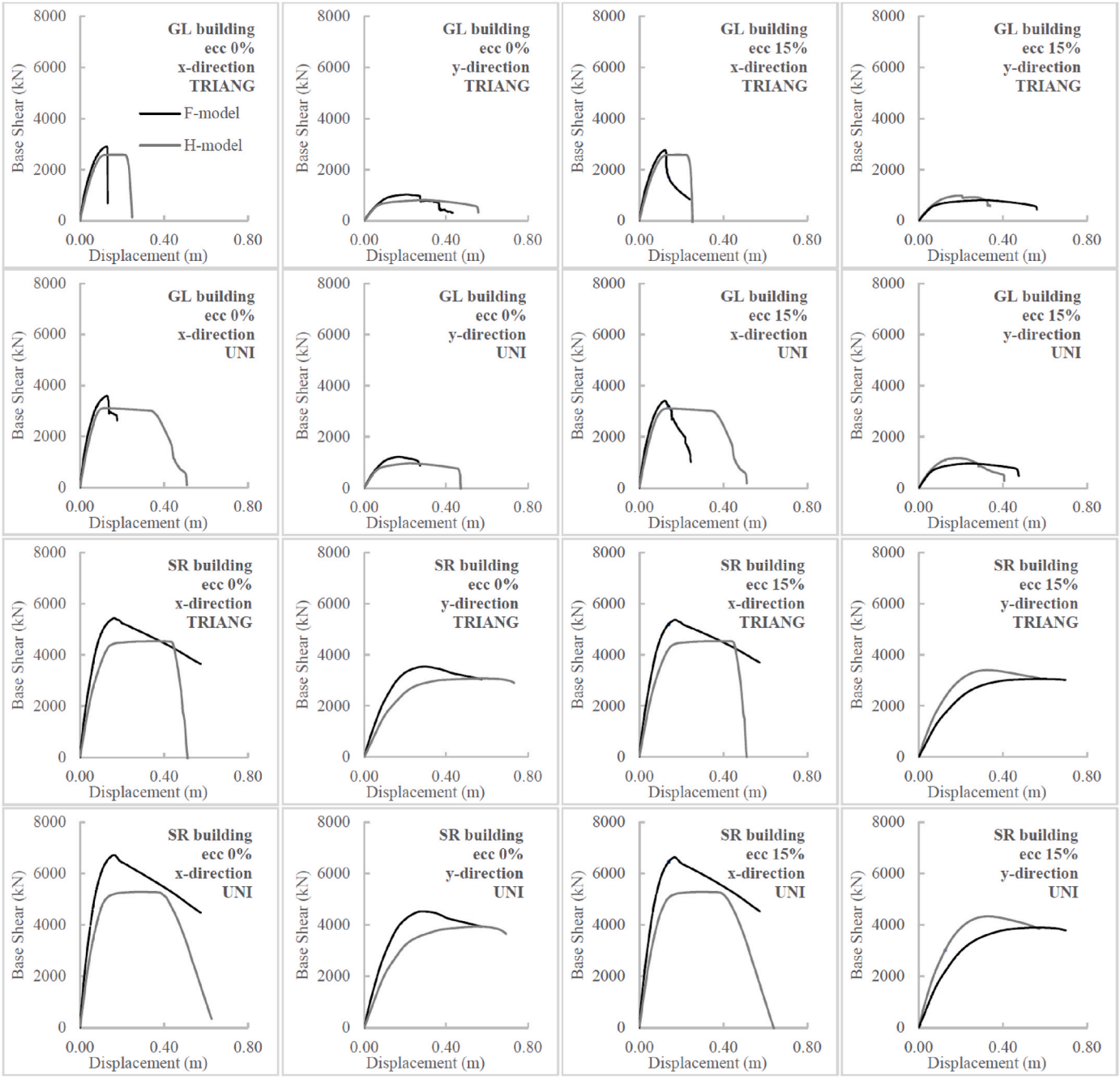

Fig. 3. Pushover curves for the four models GL-F, GL-H, SR-F and SR-H in the x- and y-directions with UNI and TRIANG load distributions and eccentricities 0% and 15%.

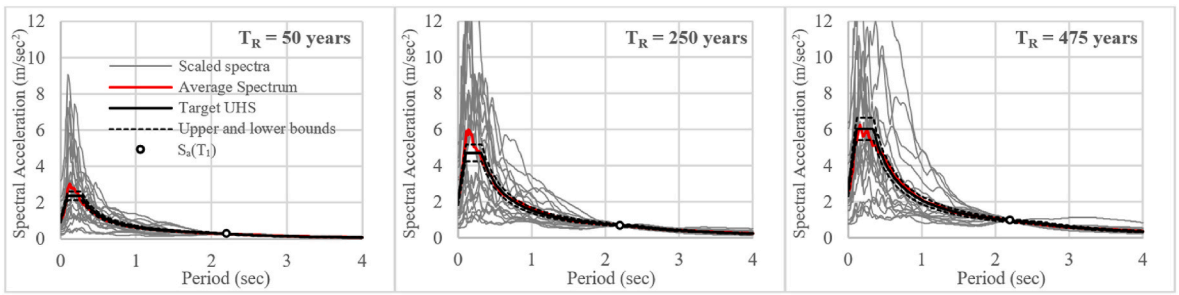

Fig. 4. Scaled geomean response spectra, average response spectrum and target UHS of the 20 record pairs selected for the GL buildings (T_1=2.2 s) for T_R = 50 yrs, T_R = 250 yrs and T_R = 475 yrs.

Table 7
RDRs of the GL-H building along the x- and y-directions for different values of e_{CM} and T_R.

GL-H building																
Dir.	T_R	e_{CM}	CM				Stiff Side					Flexible Side				
			N2–N2ext	N2-100:30	NTHA	1-(N2/NTHA)	N2	N2ext	N2-100:30	NTHA	1-(N2/NTHA)	N2	N2ext	N2-100:30	NTHA	1-(N2/NTHA)
x-direction	**50yr**	**5%**	0.19%	0.19%	0.15%	−30.29%	0.18%	0.24%	0.19%	0.17%	−5.32%	0.21%	0.21%	0.22%	0.15%	−36.76%
		15%	0.20%	0.20%	0.14%	−42.16%	0.14%	0.31%	0.17%	0.18%	22.21%	0.23%	0.23%	0.26%	0.17%	−37.37%
	250yr	**5%**	0.43%	0.43%	0.34%	−27.91%	0.39%	0.53%	0.41%	0.36%	−9.16%	0.46%	0.46%	0.48%	0.34%	−34.83%
		15%	0.45%	0.45%	0.31%	−45.04%	0.31%	0.70%	0.37%	0.37%	16.07%	0.52%	0.52%	0.58%	0.35%	−50.10%
	475yr	**5%**	0.59%	0.59%	0.47%	−24.67%	0.53%	0.73%	0.56%	0.52%	−3.27%	0.63%	0.63%	0.66%	0.48%	−31.59%
		15%	0.61%	0.61%	0.43%	−41.53%	0.42%	0.95%	0.50%	0.54%	22.06%	0.72%	0.72%	0.80%	0.51%	−41.02%
y-direction	**50yr**	**5%**	0.30%	0.30%	0.29%	−4.61%	0.27%	0.30%	0.27%	0.26%	−3.63%	0.32%	0.34%	0.33%	0.35%	6.31%
		15%	0.30%	0.30%	0.28%	−8.76%	0.21%	0.30%	0.22%	0.29%	28.33%	0.35%	0.39%	0.36%	0.37%	6.44%
	250yr	**5%**	0.78%	0.78%	0.52%	−50.90%	0.70%	0.78%	0.71%	0.45%	−57.40%	0.85%	0.89%	0.86%	0.64%	−32.73%
		15%	0.81%	0.81%	0.50%	−61.69%	0.55%	0.81%	0.58%	0.53%	−3.72%	0.95%	1.04%	0.98%	0.69%	−36.80%
	475yr	**5%**	1.07%	1.07%	0.85%	−25.61%	0.98%	1.07%	0.99%	0.73%	−33.58%	1.14%	1.22%	1.15%	1.02%	−11.99%
		15%	1.11%	1.11%	0.85%	−31.52%	0.81%	1.11%	0.85%	0.81%	0.04%	1.28%	1.44%	1.31%	1.09%	−16.70%

Table 8
RDRs of the SR-F building along the x- and y-directions for different values of e_{CM} and T_R.

SR-F building																
Dir.	T_R	e_{CM}	CM				Stiff Side					Flexible Side				
			N2–N2ext	N2-100:30	NTHA	1-(N2/NTHA)	N2	N2ext	N2-100:30	NTHA	1-(N2/NTHA)	N2	N2ext	N2-100:30	NTHA	1-(N2/NTHA)
x-direction	**50yr**	**5%**	0.31%	0.31%	0.37%	17.81%	0.28%	0.36%	0.29%	0.45%	38.05%	0.33%	0.33%	0.34%	0.38%	14.05%
		15%	0.32%	0.33%	0.34%	5.25%	0.23%	0.40%	0.25%	0.43%	46.85%	0.37%	0.40%	0.39%	0.42%	13.28%
	250yr	**5%**	0.42%	0.42%	0.53%	21.41%	0.38%	0.50%	0.40%	0.62%	37.79%	0.45%	0.45%	0.46%	0.55%	19.07%
		15%	0.43%	0.44%	0.45%	5.04%	0.31%	0.55%	0.35%	0.63%	51.03%	0.50%	0.54%	0.53%	0.55%	9.70%
	475yr	**5%**	0.58%	0.58%	0.61%	4.64%	0.53%	0.69%	0.55%	0.75%	28.59%	0.62%	0.62%	0.64%	0.64%	3.04%
		15%	0.60%	0.62%	0.57%	−5.66%	0.43%	0.76%	0.49%	0.79%	45.55%	0.69%	0.75%	0.75%	0.69%	−0.32%
y-direction	**50yr**	**5%**	0.51%	0.51%	0.55%	8.40%	0.45%	0.50%	0.46%	0.58%	22.36%	0.55%	0.59%	0.57%	0.72%	23.40%
		15%	0.53%	0.54%	0.59%	10.09%	0.33%	0.53%	0.37%	0.76%	56.57%	0.64%	0.69%	0.68%	0.80%	19.76%
	250yr	**5%**	0.69%	0.70%	0.70%	0.49%	0.60%	0.69%	0.62%	0.73%	17.83%	0.77%	0.81%	0.79%	0.89%	13.91%
		15%	0.73%	0.75%	0.73%	−0.04%	0.43%	0.73%	0.48%	1.01%	57.58%	0.89%	0.95%	0.95%	0.97%	8.01%
	475yr	**5%**	0.96%	0.96%	1.09%	12.11%	0.82%	0.96%	0.84%	0.96%	14.92%	1.07%	1.12%	1.09%	1.35%	21.15%
		15%	1.01%	1.03%	1.10%	7.93%	0.55%	1.01%	0.62%	1.05%	47.56%	1.26%	1.32%	1.33%	1.50%	15.91%

Table 9
RDRs of the SR-H building along the x- and y-directions for different values of e_{CM} and T_R.

SR-H building														
Dir.	T_R	e_{CM}	CM				Stiff Side				Flexible Side			
			N2–N2ext	N2-100:30	NTHA	1-(N2/NTHA)	N2	N2ext	N2-100:30	NTHA	1-(N2/NTHA)	N2	N2ext	N2-100:30	NTHA	1-(N2/NTHA)
x-direction	**50yr**	**5%**	0.38%	0.38%	0.32%	−17.32%	0.35%	0.52%	0.36%	0.17%	−107.27%	0.41%	0.41%	0.43%	0.34%	−19.77%
		15%	0.39%	0.39%	0.31%	−25.58%	0.28%	0.46%	0.32%	0.18%	−56.25%	0.45%	0.45%	0.49%	0.39%	−14.51%
	250yr	**5%**	0.52%	0.52%	0.43%	−20.63%	0.47%	0.70%	0.50%	0.36%	−32.28%	0.56%	0.56%	0.58%	0.46%	−20.54%
		15%	0.53%	0.53%	0.42%	−25.69%	0.38%	0.63%	0.45%	0.37%	−3.04%	0.61%	0.62%	0.67%	0.52%	−16.57%
	475yr	**5%**	0.69%	0.69%	0.59%	−16.17%	0.63%	0.93%	0.66%	0.52%	−22.81%	0.73%	0.73%	0.76%	0.62%	−18.62%
		15%	0.71%	0.71%	0.58%	−20.97%	0.52%	0.84%	0.60%	0.54%	3.50%	0.81%	0.83%	0.88%	0.69%	−16.16%
y-direction	**50yr**	**5%**	0.63%	0.63%	0.58%	−9.96%	0.56%	0.63%	0.57%	0.26%	−113.61%	0.69%	0.73%	0.71%	0.71%	1.85%
		15%	0.67%	0.67%	0.57%	−17.75%	0.42%	0.67%	0.45%	0.29%	−45.85%	0.81%	0.87%	0.84%	0.79%	−1.62%
	250yr	**5%**	0.86%	0.86%	0.75%	−15.53%	0.74%	0.86%	0.76%	0.45%	−65.89%	0.96%	0.99%	0.98%	0.91%	−5.95%
		15%	0.92%	0.92%	0.74%	−24.80%	0.54%	0.92%	0.58%	0.53%	−1.89%	1.13%	1.19%	1.18%	1.00%	−12.69%
	475yr	**5%**	1.15%	1.15%	0.91%	−26.47%	1.00%	1.15%	1.02%	0.73%	−35.94%	1.28%	1.32%	1.30%	1.12%	−14.10%
		15%	1.23%	1.23%	0.91%	−35.35%	0.70%	1.23%	0.77%	0.81%	13.71%	1.51%	1.59%	1.58%	1.23%	−22.96%

large plan asymmetry. As expected, the three modes are uncoupled (x-direction, z-rotation and y-direction) for $e_{CM} = 0\%$ with the degree of coupling increasing with e_{CM}. Regarding the comparison between the outcomes of the F and H modelling approaches, it should be noted that the two modelling strategies follow different criteria to define the members' initial stiffness, as explained in the previous section. Hence, it is not surprising that the initial periods of the same building modelled with two different approaches are different. Nonetheless, the GL-F and GL-H periods in the y direction are similar. In this case, most likely, the initial stiffness of the Haselton curve (secant to 40% the yield moment) in the H model produces stiffnesses (mainly in the columns, since there are no beams in the considered direction) that are comparable to those of the fibre section model.

The first vibration periods of the GL structure reflect the fact that the load carrying beams are aligned in the y-direction, the unidirectional slabs are oriented in the y-direction and there are no beams in the y-direction with the exception of the two perimeter beams. Thus, there are 4 frames in the x-direction and 2 perimeter frames only in the y-direction, with a first vibration period much higher in the y-than in the x-direction. On the other hand, the SR structure has the same number of frames in the two directions and thus similar first vibration periods in the two directions.

According to Ref. [38], a building is classified as torsionally stiff or flexible depending on the ratio Ω between the uncoupled torsional frequency ω_θ and the uncoupled lateral frequency ω_h. These frequencies are those of the "corresponding torsionally balanced system", which is obtained shifting the centres of mass of the analysed building into the centres of stiffness of its structure. Given the symmetry of the analysed structures with respect to the geometric centre of the floor, the centres of stiffness are lined up along a vertical line connecting the geometric centres of the floors. If $\Omega > 1$, the response is mainly translational and the structure is defined as torsionally stiff; conversely, if $\Omega < 1$ the response is affected to a large degree by torsional behaviour. For each analysed asymmetric building, the corresponding torsionally balanced system coincides with the one with $e_{CM} = 0\%$. Hence, considering that the ratio of the frequencies is the inverse of the ratio of the periods, Table 2 through Table 5 show that $\Omega_x < 1$ and $\Omega_y > 1$ for all the case study buildings, they can thus be considered torsionally flexible in the x-direction and torsionally stiff in the y direction.

3. Non-linear analyses of the case study buildings

PO analyses are carried out using the N2 method, the N2 method plus the 100:30 combination rule and the N2ext method. The results of NTHAs are used as reference.

3.1. Non-linear static analyses

Two separate PO analyses are carried out pushing the structures in the x and y directions. For the N2 method only, the results are then combined using the 100:30 directional combination rule. For the N2ext method the combination rule is already considered in the RSA used for the method extension.

3.1.1. Brief recap of the N2 method

The N2 method is a well-established analysis method of analysis, used both in practice and in research. Its basic principles are recalled in Fig. 2. According to the N2 method [2,39–42], the structure is pushed with an incremental constant-shape force distribution and the nonlinear *F-D* curve is recorded, where *F* is the base shear and *D* is the displacement of the roof CM (Fig. 2a and b). At least two load shapes are typically required by the design codes. The basic ones are typically an inverted triangle, labelled TRIANG (that represents an approximation of the first mode shape in the loading direction) and a mass proportional load vector, labelled UNI (that represents the inertia forces acting on the frame if a soft storey forms at the ground level and corresponds to a

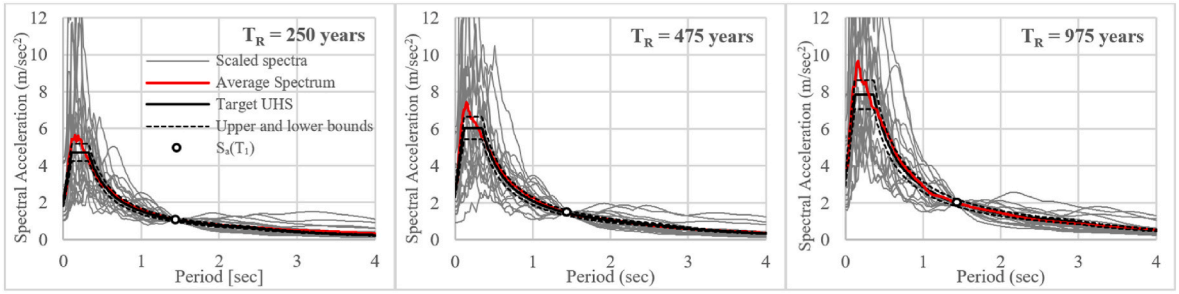

Fig. 5. Scaled geomean response spectra, average response spectrum and target UHS of the 20 record pairs selected for SR-F building (T_1 = 1.45 s) for T_R = 250 yrs, T_R = 475 yrs and T_R = 975 yrs.

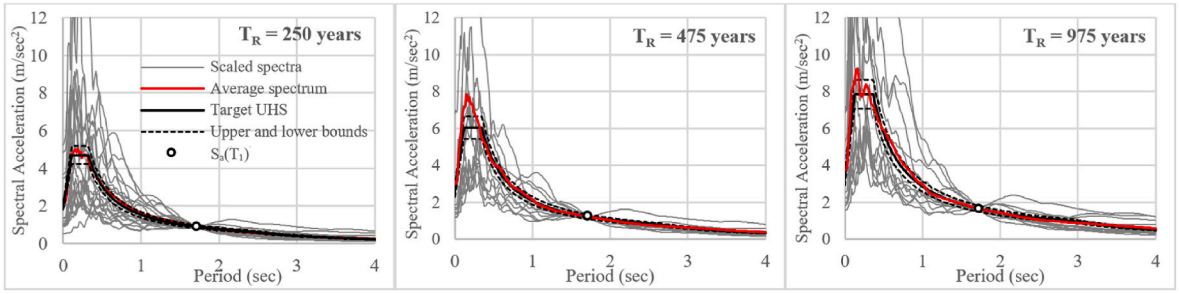

Fig. 6. Scaled geomean response spectra, average response spectrum and target UHS of the 20 record pairs selected for SR-H building (T_1 = 1.72 s) for T_R = 250 yrs, T_R = 475 yrs and T_R = 975 yrs.

uniform vector along the building height in case of equal masses at all storeys). Each *F-D* curve is then transformed into the *F*-D** curve of an equivalent Single-Degree-Of-Freedom (SDOF) using a transformation factor Γ. The nonlinear curve is thus transformed into an equivalent bilinear curve (Fig. 2c and d). The basic N2 method is based on a number of assumptions that explain some of its limitations: it was originally developed for plane frames and it rests on the strong assumption that the displacement response shape is proportional to that of the loading vector. The *F*-D** curve is a capacity curve. It is compared with the demand curve in an Acceleration-Displacement (AD) plane by superimposing the nonlinear capacity curve (transformed in an AD curve) with the elastic pseudo-acceleration spectrum S_a (typically computed for 5% damping) of the design earthquake (Fig. 2e, f and g). The elastic spectrum should be transformed into an inelastic spectrum, but this operation is simplified to obtain the so-called design (or target) point, that is the displacement demand D^*_t for the given design earthquake. The equivalent SDOF D^*_t is then transformed back into the roof target displacement D_t of the MDOF system through Γ (Fig. 2h). Each of these transformations (MDOF to SDOF and back, simplification of the equivalent nonlinear SDOF) introduce additional approximations.

Fig. 3 shows the capacity curves for the four models GL-F, GL-H, SR-F and SR-H in the x- and y-directions with UNI and TRIANG load distributions and eccentricities 0% and 15%. As expected, the SR building, that was designed according to an older seismic code, has a higher capacity than the GL building, that was designed for gravity loads only. Furthermore, the curves in the y-direction are more ductile and less resistant than those in the x-direction because there are no interior transverse beams in the GL building y-direction, while all interior beams in the SR building y-direction are flat. The initial stiffness of the Haselton curve (secant to 40% the yield moment) in the H models produces in most cases curves with lower stiffness than that of the F models. This difference leads to target displacements Dt generally higher for the H models. For additional details on the PO analyses carried out with the F and H models, see Ref. [43], that presents an in-depth discussion of the two modelling strategies and compares the structural demands at different limit states.

Current design codes [3,4,44–46] prescribe the application of a combination rule for the results of the original N2 method to account for the simultaneous application of the two seismic horizontal components. According to EC8 [4] either the SRSS or the 100:30 combination rule can be applied. Although several studies have been published on the application of PO analyses to irregular 3D structures subjected to bidirectional ground motions (among others [10,17,18,47,48]), only few apply a combination rule. The 100:30 combination rule is applied in this study to assess its impact on the demand estimation computed with the N2 method.

3.1.2. *The extended N2 method*

Starting from the original N2 method that applies to plan regular buildings with the first two modes (fundamentally uncoupled) in the x and y directions, the N2ext method [8,9] was proposed to account for the non-negligible building rotations around the vertical z axis of in plan-irregular 3D buildings. The seismic demand in terms of displacements and storey drifts is found by combining the results of the initial PO analyses with those of a RSA. More specifically, in this study PO analyses are carried out on the 3D models by applying two lateral load patterns at the floors' CMs. Following FEMA 356 [44] and the Italian design code [3] the two load distributions are UNI and TRIANG. In each loading direction, the response is monitored in three points: the CM, the flexible side (i.e. the rectangle side closer to the CM), and the stiff side. The steps of the N2ext method are summarized as follows:

a) The original N2 [1,2] PO procedure is used to find the top displacement demand D_t (one for each direction). For each direction, the larger of the two displacements in the positive and negative directions is used. The step is carried out for both load shapes.
b) A standard RSA of the 3D structural models (after application of the gravity loads) is carried out using a 5% damping elastic design spectrum (for details, see §3.1.2). The demands for all modes are combined with the CQC rule, and the demands from the two horizontal spectra are spatially combined according to the SRSS rule. The

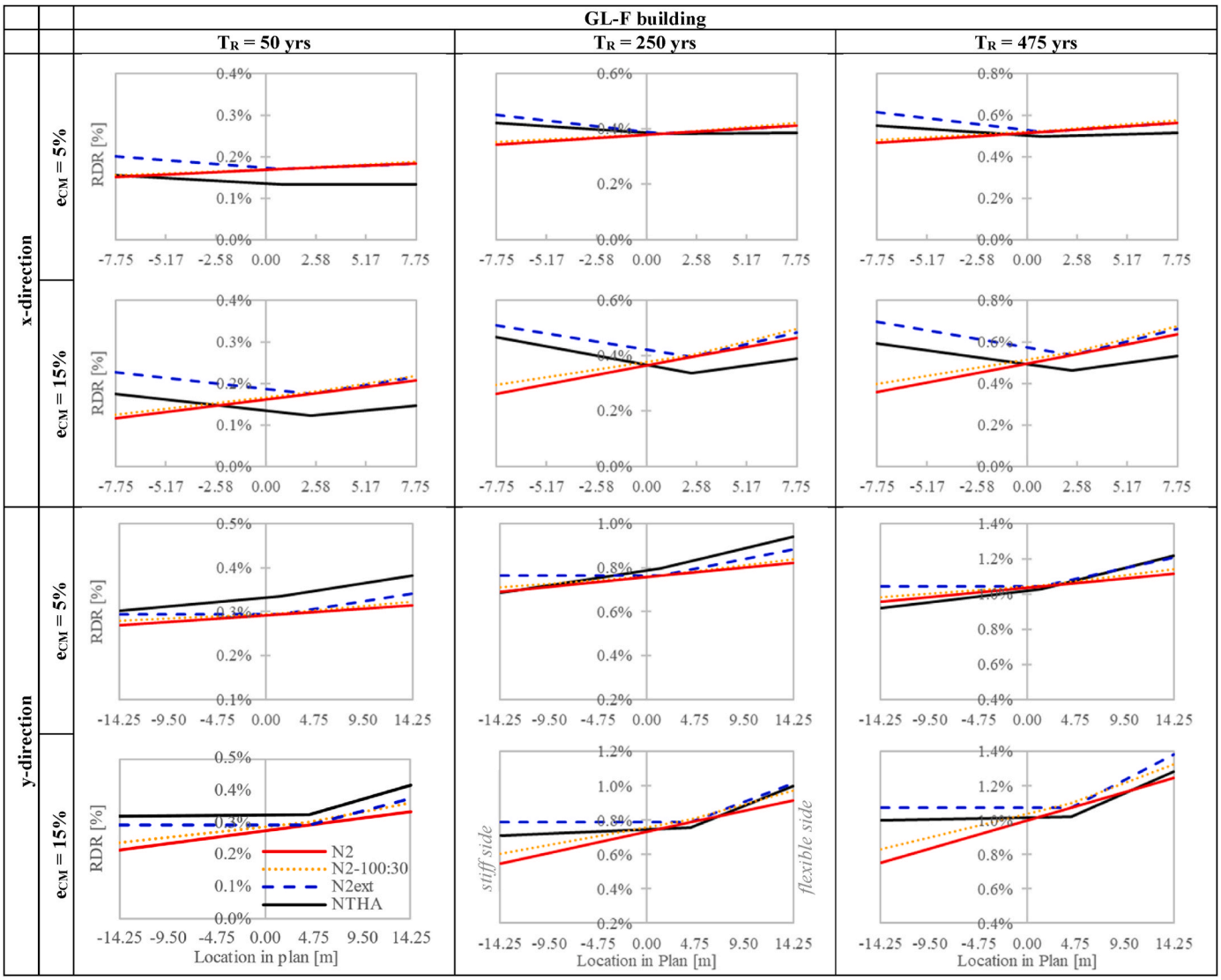

Fig. 7. GL-F building model RDRs for e_{CM} = 5% and e_{CM} = 15%.

roof displacements in the x and y directions at different points on the roof are normalized with respect to the roof displacement of CM.

c) The demands computed in step a) are updated by applying correction factors. For any roof point different from the CM, the correction factor is the ratio between the point normalized displacement computed by RSA and PO analyses. For a given analysis (RSA or PO), the normalized roof displacement is the point displacement divided by the roof CM displacement. If the RSA normalized roof displacement is less than 1.0 the value 1.0 is used, i.e. de-amplification due to torsion is discarded (as suggested in the original method [9]). The correction factors depend on the point plan location. In some cases, the application of the above procedure can produce correction factors on the flexible side lower than 1.0, thus unconservative with respect to the N2 method. The authors in these cases used a coefficient factor equal to 1.0.

Note that in the N2ext method, the demands from the RSA along the two structure reference axes are spatially combined with the SRSS rule. Therefore, this method considers the bidirectionality of the seismic input and for this reason the 100:30 combination rule prescribed by Ref. [3] was applied only to the N2 method and not to the N2ext method.

3.2. Nonlinear time history analyses

NTHAs are carried out by applying a set of selected ground motion records to the nonlinear structural models. The F and H models use different Rayleigh damping models. The F models use 2% damping (at the first and third mode frequency) with full initial stiffness. The H models use 5% damping for the same frequencies, but damping is applied only to the elastic elements to avoid spurious damping forces that develop after yielding in the plastic hinges [49]. It is assumed that 2% damping in all elements (model F) is comparable to 5% in the elastic elements only (model H). To compare the effects of the two damping approaches for the two different models, the NTHAs later discussed in the paper were repeated with and without damping. It was observed that the demand ratios (mainly, the interstorey drifts) obtained with the F and H models with and without damping are comparable thus confirming that the two different damping models have similar effects on the two models.

3.2.1. Ground motion record selection

The ground motion record selection was carried out for three different hazard levels. The return periods are different for the two buildings as the GL building is expected to fail for lower intensities. For the GL and SR buildings, return periods of 50, 250, 475 yrs and 250, 475,

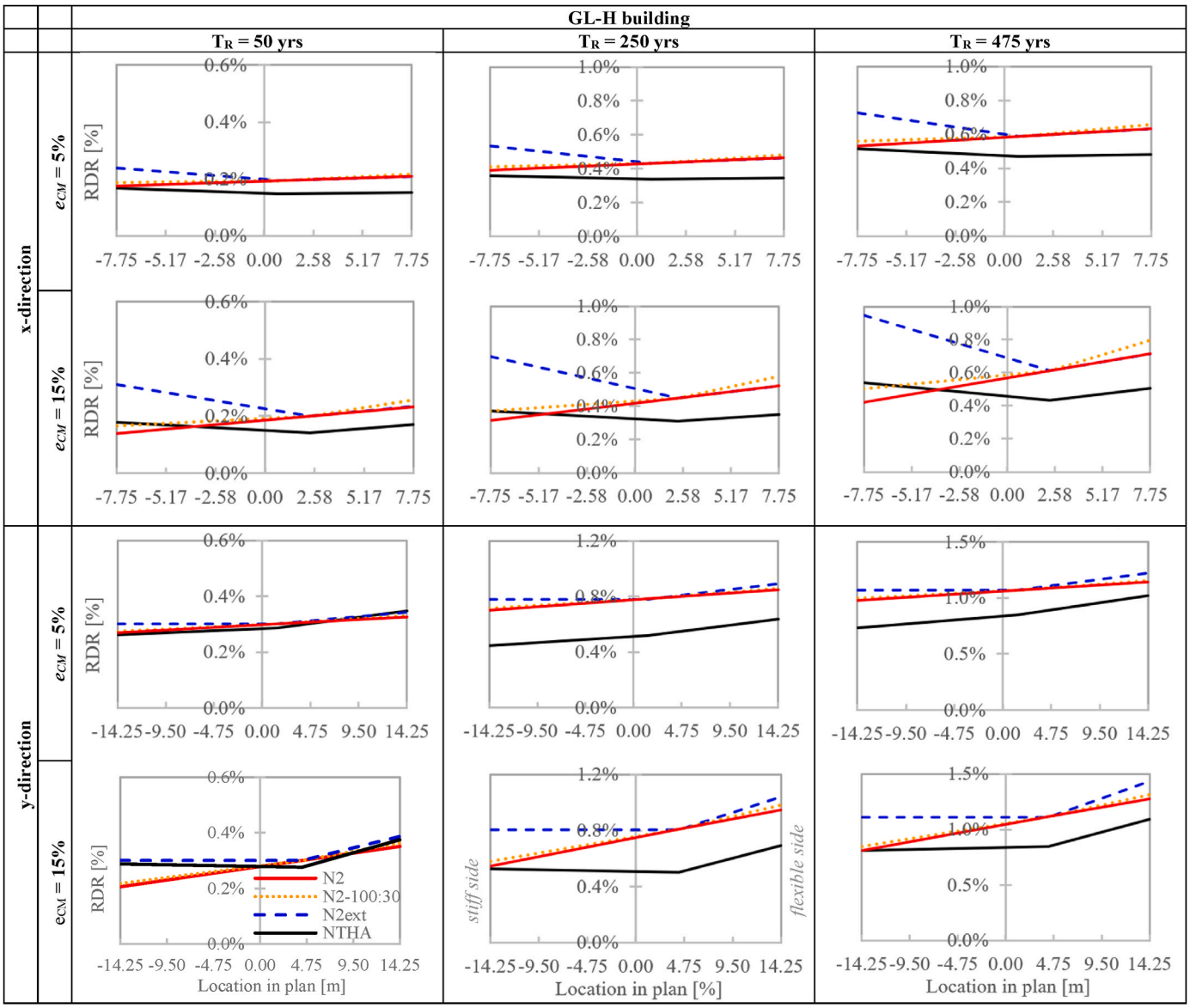

Fig. 8. GL-H building model RDRs for e_{CM} = 5% and e_{CM} = 15%.

975 yrs were considered, respectively. For both buildings, the reference site is L'Aquila, AQ-Italy, 42.350° latitude and 13.399° longitude, on rock soil. Strictly speaking, there are no GL buildings in L'Aquila as the site was classified as seismic before WWII. The assumption is however valid as there are several areas in Italy that were originally classified as non-seismic areas in the '70s but have today a seismic hazard similar to that of L'Aquila. The ground motion records were selected from two databases: the European Strong-motion Database ESD [50] and the Engineering Strong-Motion database ESM [51]. Only the two orthogonal horizontal components were considered for each selected ground motion.

Following Beyer and Bommer [52], if $S_{ax}(T)$ and $S_{ay}(T)$ are the response spectra of the two ground motion components, a single geometric mean spectrum $S_a(T)$ is found as $S_a(T) = \sqrt{S_{ax}(T) \cdot S_{ay}(T)}$. The spectra of all selected ground motion record pairs are then scaled to the Uniform Hazard Spectrum (UHS) target spectral acceleration $S_{a,UHS}(T_1)$ at the first vibration period T_1 of a given structure [53]. For each ground motion record pair, a single scale factor SF is used for both horizontal components, so that $SF = S_{a,UHS}(T_1)/S_a(T_1)$. The unrealistic use of high scale factors was avoided, as suggested in Refs. [54–57], by imposing $SF < 5$. For each structure and for a given hazard, 20 recorded ground motion record pairs were selected to comply with the EC8 spectrum compatibility criterion [4] that states that in the period range $0{,}2T_1$ - $2T_1$, the mean elastic spectrum of the 20 geometric means $S_a(T)$ should be above 90% of the corresponding UHS. Though no upper bound is prescribed in Ref. [4], a 110% upper bound was imposed here. Given two buildings, two models (F and H) and three hazard levels for each building, a total of 12 groups of 20 ground motion record pairs should be selected. However, since T_1 of GL-F an GL-H are very similar (Tables 2 and 3), the total number of groups was reduced to 9.

Fig. 4 shows the scaled geometric response spectra of the three groups of 20 ground motion record pairs (corresponding to return periods T_R = 50, 250 and 475 years) for the GL buildings. Reported in red is the average response spectrum. The target UHS is shown in solid black, with $S_{a,UHS}(T_1)$ and T_1 = 2.2 s. The seismological features of the records (Database, Code of the Station, Name, Earthquake Date, Time, Moment Magnitude M_w, Epicentral Distance R, Site Class and Scale Factor) are reported in Table A7, Table A8 and Table A9 of the Appendix.

Figs. 5 and 6 report the same information for the two groups of records selected for buildings SR-F and SR-H, respectively. As previously pointed out, given the expected higher strength of the SR building with respect to the GL building, T_R = 250, 475 and 975 yrs. The seismological

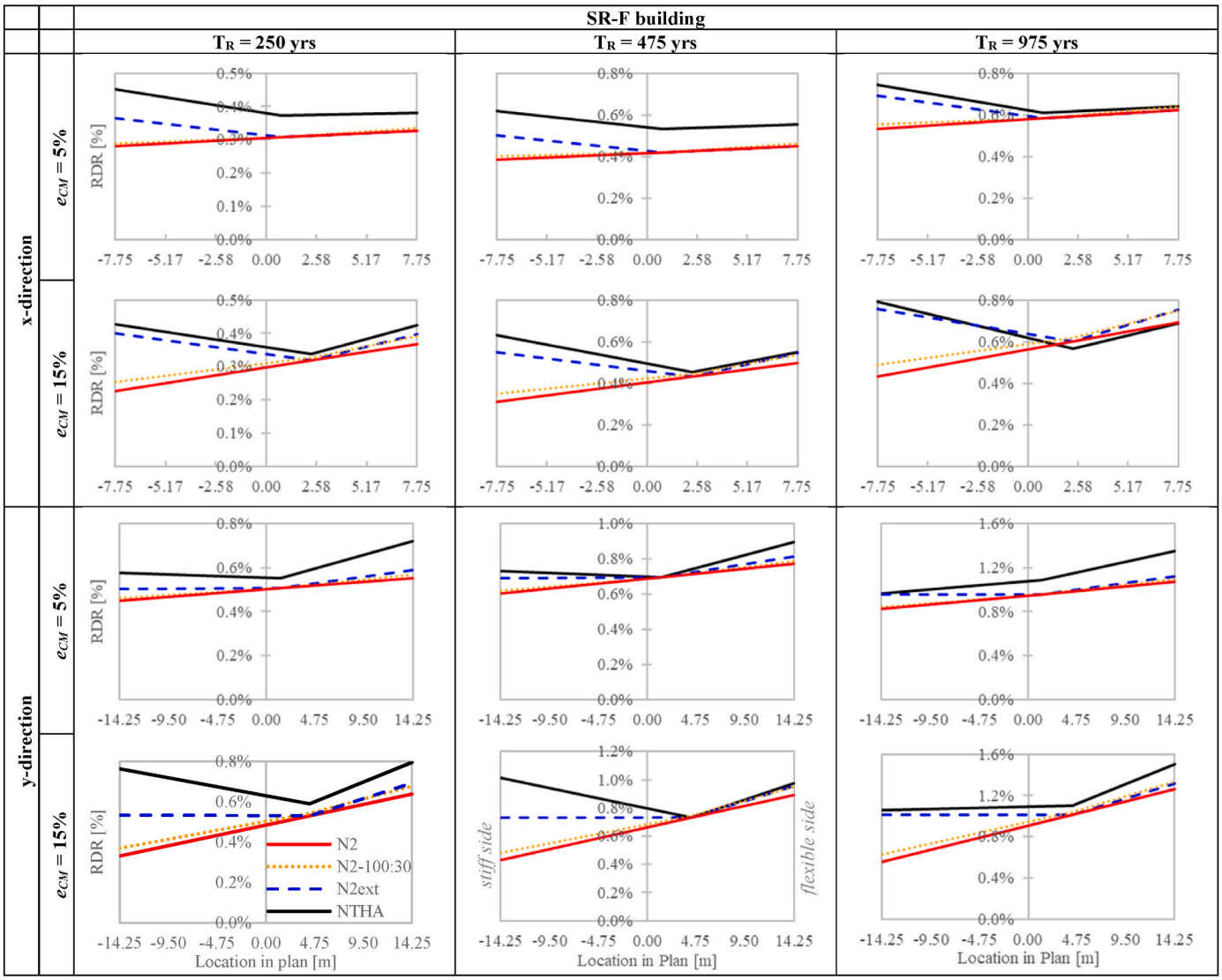

Fig. 9. SR-F building model RDRs for e_{CM} = 5% and e_{CM} = 15%.

features of the records are reported in the Appendix (from Table A10 to Table A15).

4. Results and discussion

The results of the PO and NTHAs are reported and discussed here using two Engineering Demand Parameters (EDPs): Roof Drift Ratio (RDR = top floor reference point displacement/building height) and Interstorey Drift Ratio (IDR = interstorey reference point displacement/storey height). While the IDRs are a direct measure of the building deformations, the RDR is the global EDP used in the development of the N2 method and is thus deemed important to compare the RDR demands of (original and extended) N2 vs NTHAs.

4.1. Roof Drift Ratios

Fig. 7 through Fig. 10 show the RDRs obtained for all four building models and all hazard levels. Only e_{CM}=5% and e_{CM}=15% are considered. Each figure reports 12 plots, organized in 3 columns and 4 rows: i) the three columns refer to the different hazard levels considered for each building model (T_R = 50, 250 and 475 yrs for the GL building and T_R = 250, 475 and 975 yrs for the SR building); ii) the first and second rows report the results in the x-direction for e_{CM}=5% (small eccentricity) and e_{CM}=15% (large eccentricity), respectively; iii) the last two rows indicate the results in the y direction. All plots report on the vertical axis the RDR and on the horizontal axis the in-plane coordinate orthogonal to the push direction. Each plot compares four curves, mainly the RDR demand found with the N2 method, the N2 method plus the 100:30 combination rule and the N2ext method, in addition to the RDR estimated by the NTHAs. In the last case, following EC8 and other design codes, the EDP (the RDR in this case) is found as the average of the largest EDP values (in absolute value) found in the 20 NTHAs. All curves report three points - the RDR of the end sides and that of the CM - connected by straight lines. They are all piecewise linear (except for the red N2 method curves that are straight because of the floor diaphragm constraint) with a change of inclination at the CM. Figs. 7 and 8, Figs. 9 and 10 show the results for the GL-F, GL-H, SR-F and SR-H building models, respectively. The corresponding RDR values are reported in Table 6, Table 7, Tables 8 and 9, respectively. They were all obtained with the TRIANG load shape whose demands are higher than those obtained with the UNI load shape. In addition to the results of the N2, N2ext, N2-100:30 and NTHA methods, Table 6 through 9 report the percentage differences (1-N2/NTHA) between the N2 and the NTHA methods for CM, stiff side and flexible side.

Since the plan distribution of RDR provided by the N2 method is linear, it cannot replicate that provided by NTHAs independently of the

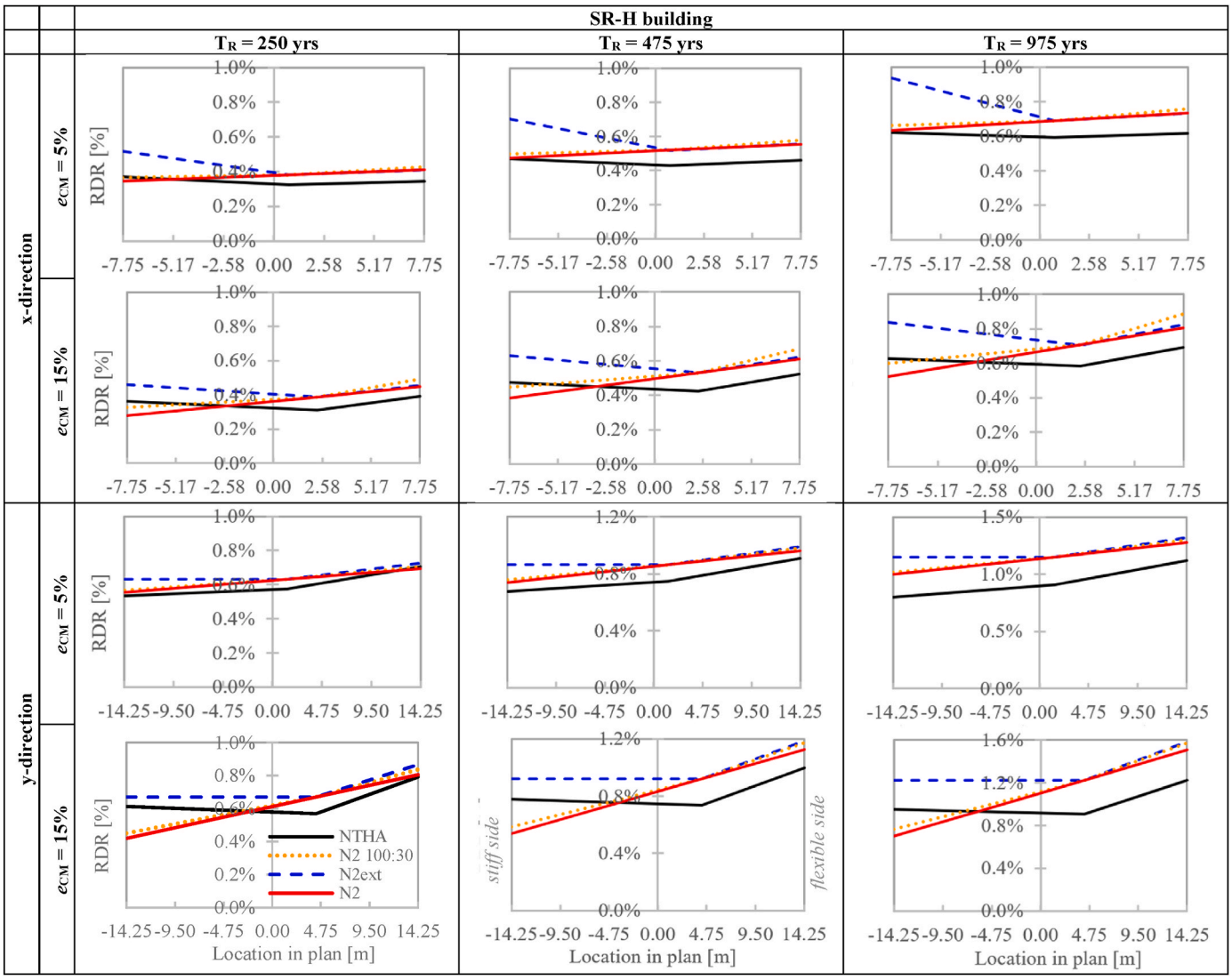

Fig. 10. SR-H building model RDRs for e_{CM} = 5% and e_{CM} = 15%.

numerical model. The scatter between the results obtained by N2 and NTHAs is often small for buildings with small eccentricity. However, it significantly increases when the e_{CM} becomes large due to the markedly non-linear shape of the RDR plan distribution obtained by NTHAs. The difference between the RDRs obtained by the N2 method and the NTHAs is quite different at the two buildings' sides. In most cases, the RDRs of the flexible side obtained by the N2 method and the NTHAs are similar even for buildings with large eccentricity. On the other hand, the inability of the N2 method to replicate the plan distribution of the RDRs provided by NTHAs negatively reflects on the prediction of the RDR of the stiff side of the buildings, which can be largely underestimated by the N2 method. For instance, regardless of the hazard level, the x-direction RDR of the stiff side of the SR-F building with e_{CM}=15% predicted by the N2 method is approximately half of the RDR of the NTHAs (Fig. 9, Table 8). The underestimation is smaller but still significant, about 30%, for the y direction RDR of the stiff side of the SR-H building with e_{CM}=15% (Fig. 10, Table 9). Finally, the largest underestimation, about 60%, is recorded for the y direction RDR of the stiff side of the SR-F building with e_{CM}=15% for T_R = 250 and 475 yrs (Fig. 9, Table 8).

The directional combination rule applied to the N2 method (the 100:30 rule in this case, but similar results should be expected for the SRSS rule) has a negligible effect on the prediction of the RDR. Independently of the numerical model, type of design (GL or SR), eccentricity e_{CM} and return period T_R, the RDR plan distribution predicted by the 100:30 rule is almost superimposed to that obtained by the N2 method alone and it still strongly underestimates the RDR of the stiff side of the building by NTHAs. It is concluded that the introduction of the 100:30 rule does not produce any improvement in the prediction of the RDR.

The N2ext method adjusts the plan distribution of RDR in plan and produces shapes that are closer to those obtained by NTHAs. The flexible side RDR is not modified with respect to that provided by the other two non-linear static methods of analysis. On the other hand, the stiff side RDR is amplified until it becomes larger than that of CM and in any case never smaller. This improves the prediction of the rigid side RDR (both in the x and y direction) in all cases and makes the extended N2 method much more effective than the original N2 method. In most cases the N2ext method eliminates the underestimation (Figs. 7, Figs. 8 and 10) and significantly reduces it in the other few cases (Fig. 9).

In some cases, the N2 method significantly overpredicts the RDR of the CM with respect to the NTHAs. The differences depend on two main reasons. The first is the variability in the RDR estimation with the PO method predicted by the F and H models, which can in a few cases be significant. Indeed, the equivalent SDOF systems of the F and H models may have different stiffness and this affects the target displacements and thus the predicted responses. As indicated in Section 3.1.1, in most cases the H-models produce target displacements D_t higher than those of F

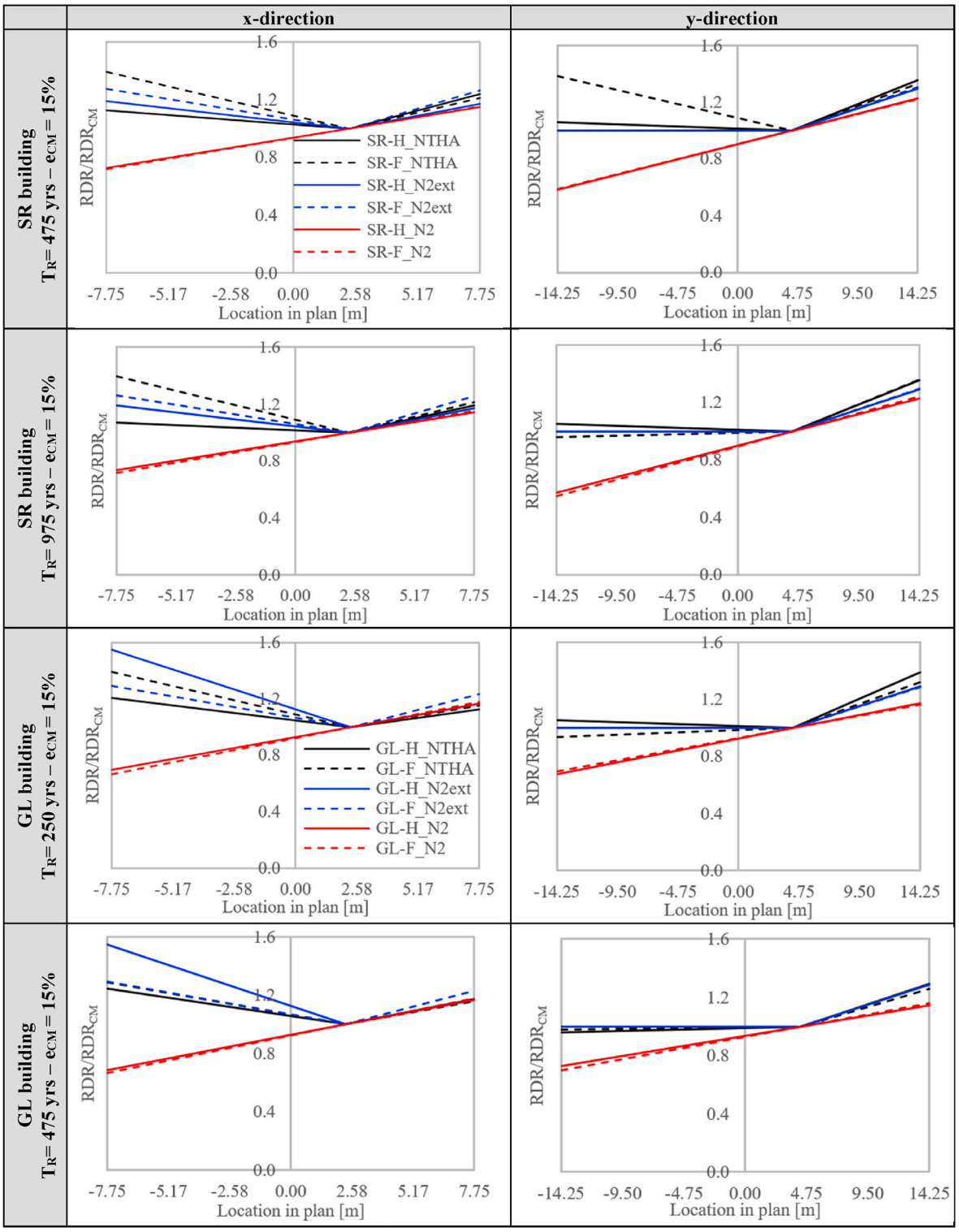

Fig. 11. RDRs normalized with respect to the CM RDR for SR building with T_R = 475 yrs (first row), SR building with T_R = 975 yrs (second row), GL building with T_R = 250 yrs (third row) and GL building with T_R = 475 yrs (fourth row). All cases refer to e_{CM} = 15%.

models due to the different modelling assumptions. The second reason is the influence of the ground motion selection on the RDR estimation by NTHAs. The ground motion selection used in this paper is presented in section 3.2.1, but other procedures can be followed for the ground motion selection or for the derivation of simulated [58] or artificial [59] ground motions. The variability in the input ground motions strongly affects the scatter of the EDPs' demands [60–62].

The overestimation of the RDR of the CM for the N2 method with respect to the NTHAs explains the overestimation of the RDR of the two sides of the building that is observed in some cases for the N2ext method. Indeed, even though the N2ext method accurately replicates the RDR plan distribution shape of the NTHAs, the N2ext does not (and cannot) improve the prediction of the CM displacement. Hence, the same overestimation of the CM displacement is obtained at the two sides of the building when the N2ext method is applied. More specifically, the maximum percentage difference between the CM RDRs from the N2 and

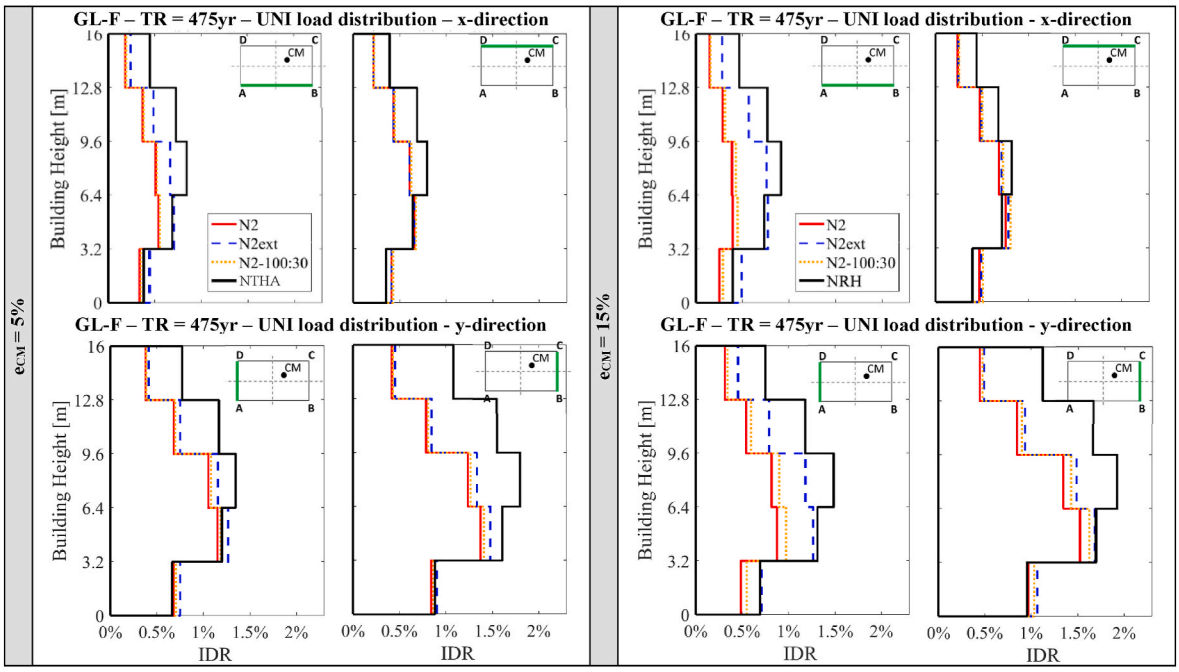

Fig. 12. GL-F building model: IDRs for e_{CM} = 5% (left) and e_{CM} = 15% (right) for T_R = 475years (UNI load pattern).

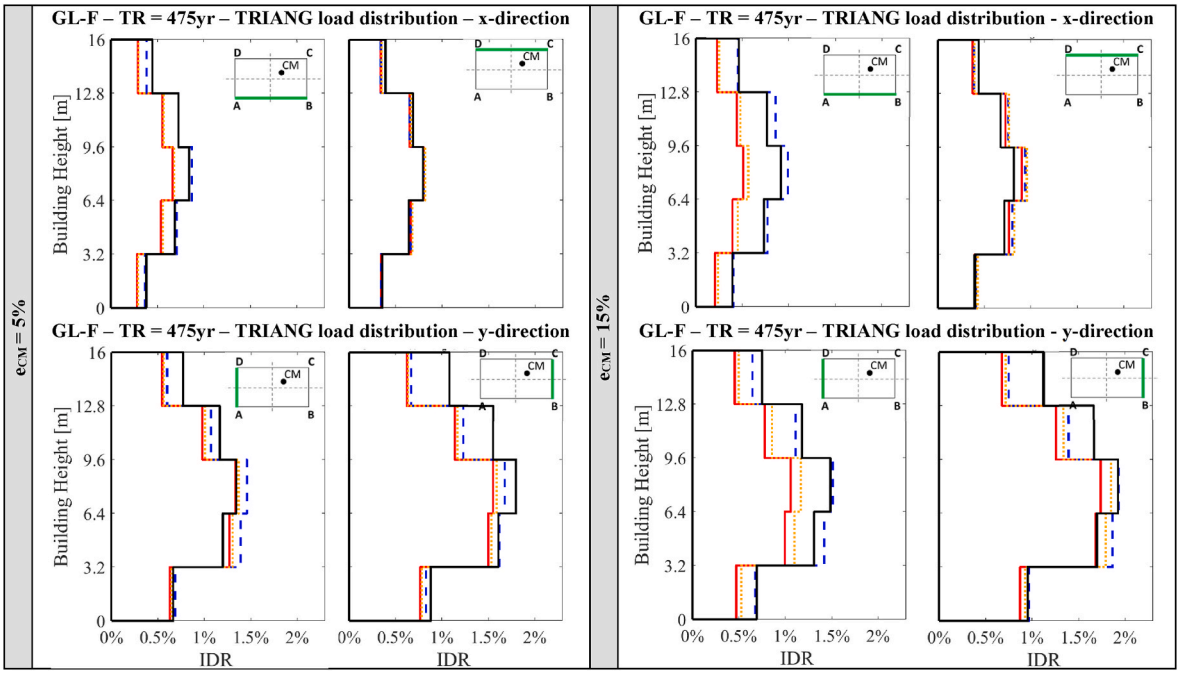

Fig. 13. GL-F building model: IDRs for e_{CM} = 5% (left) and e_{CM} = 15% (right) for T_R = 475years (TRIANG load pattern).

the NTHA methods is about 62% and is obtained for the GL-H building in the y direction of e_{CM}=15% for T_R = 250 yrs (Fig. 8, Table 7).

While the N2ext method does not change the CM RDR prediction, it affects the RDR on the stiff side of the building plan. To assess the impact of this correction, Fig. 11 shows the same results of Fig. 7 through Fig. 10 with the RDR normalized with respect to the CM RDR (different for each curve). Each plots compares the results for the two models (F and H), the N2 and the N2ext methods and the NTHAs. For the SR building (top two rows) the results refer to the highest hazards (T_R = 475 and 950 yrs), for the GL building the third row reports the results for T_R = 475 yrs. The left column refers to the x-direction, the right one to the y-direction.

More specifically, the eight plots in Fig. 11 refer to the x- and y-directions of the SR building with T_R = 475 yrs and T_R = 975 yrs and the GL building with T_R = 250 yrs and T_R = 475 yrs, respectively. The plots show the effectiveness of the N2ext correction on the stiff side, where the increase in RDR can be significant.

4.2. Interstorey Drift Ratios

Given the large amount of data available, a selection of the most representative results was necessary. The T_R=475yrs case only is discussed. Figs. 12 and 13 show the IDR results of building model GL-F for

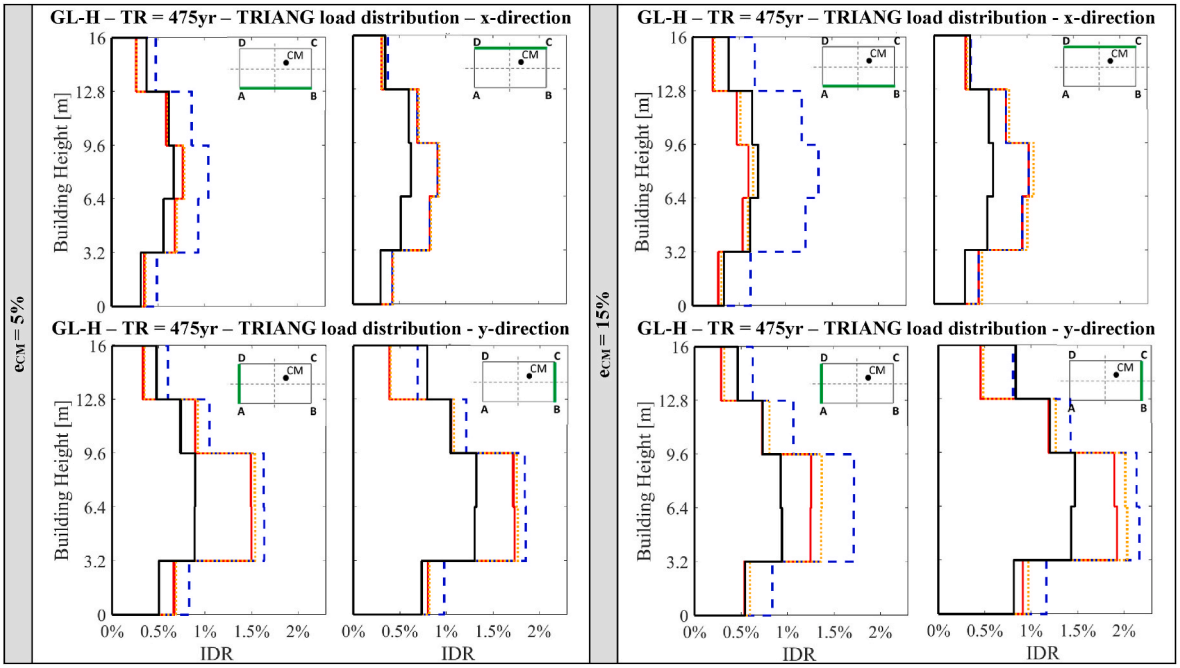

Fig. 14. GL-H building model: IDRs for e_{CM} = 5% (left) and e_{CM} = 15% (right) for T_R = 475years (TRIANG load pattern).

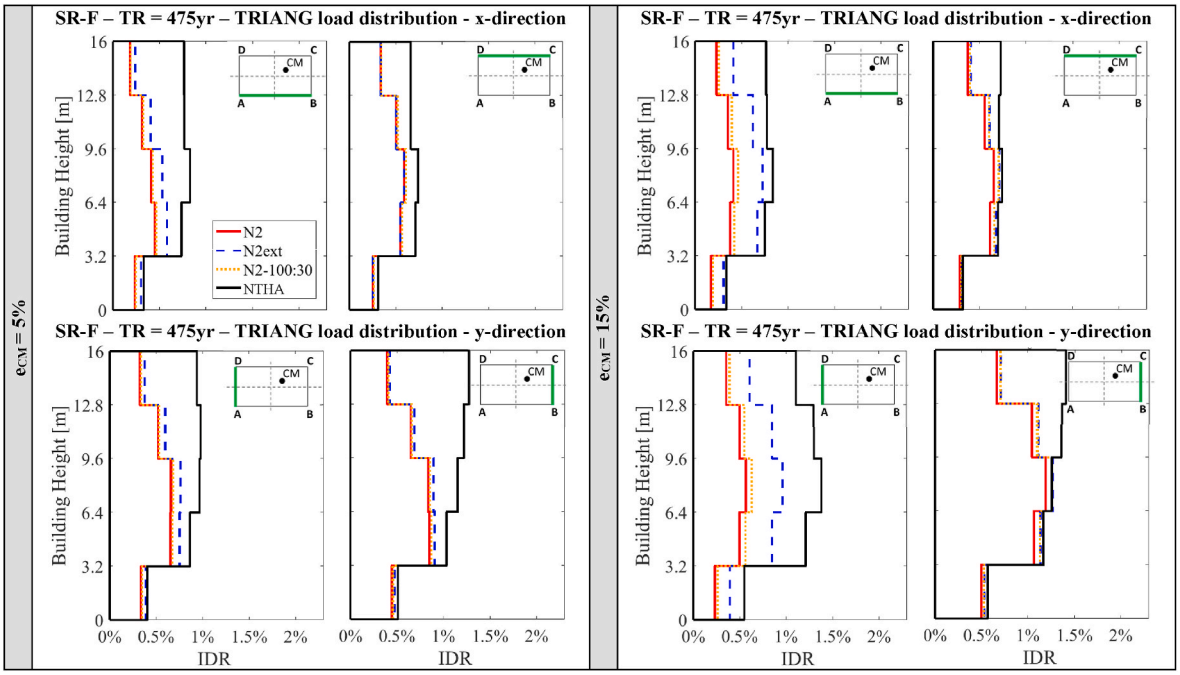

Fig. 15. SR-F building model: IDRs for e_{CM} = 5% (left) and e_{CM} = 15% (right) for T_R = 475years (TRIANG load pattern).

UNI and TRIANG load shapes, respectively. The four plot groups to the left and to the right refer to e_{CM}=5% and e_{CM}=15%, respectively. Each of the four plots refers to one of the four building sides (indicated in green in the legend drawing). The top and bottom rows refer to PO in the x- and y-direction, respectively. Each plot reports the IDR distribution over the buildings' height obtained by means of the N2 method, the N2 method with the 100:30 combination rule, the N2ext method and the NTHA. In almost all cases the demand from the TRIANG load shape is higher to that of the UNI load shape. In few cases, the bottom storey demand from UNI is higher than the TRIANG, but the differences are minor. For this reason, the discussion is limited to the results for all models loaded by the TRIANG load shape. Fig. 12 presents the IDR obtained by the UNI load shape. Figs. 13, 14, 15 and 16 illustrate the results obtained by the TRIANG load shape for the GL-F, GL-H, SR-F and SR-H models, respectively.

For both the GL and SR buildings, the y-direction IDRs are significantly higher than those in the x direction. This is typical for buildings of the 70s and 80s that present one direction that is much more flexible that the other. Furthermore, it is observed that in most cases, the maximum IDR demand computed by NTHAs is recorded at the third storey. In the few cases where this does not happen (for example side BC in model SR-F) the IDR demand at the third storey is comparable to the maximum

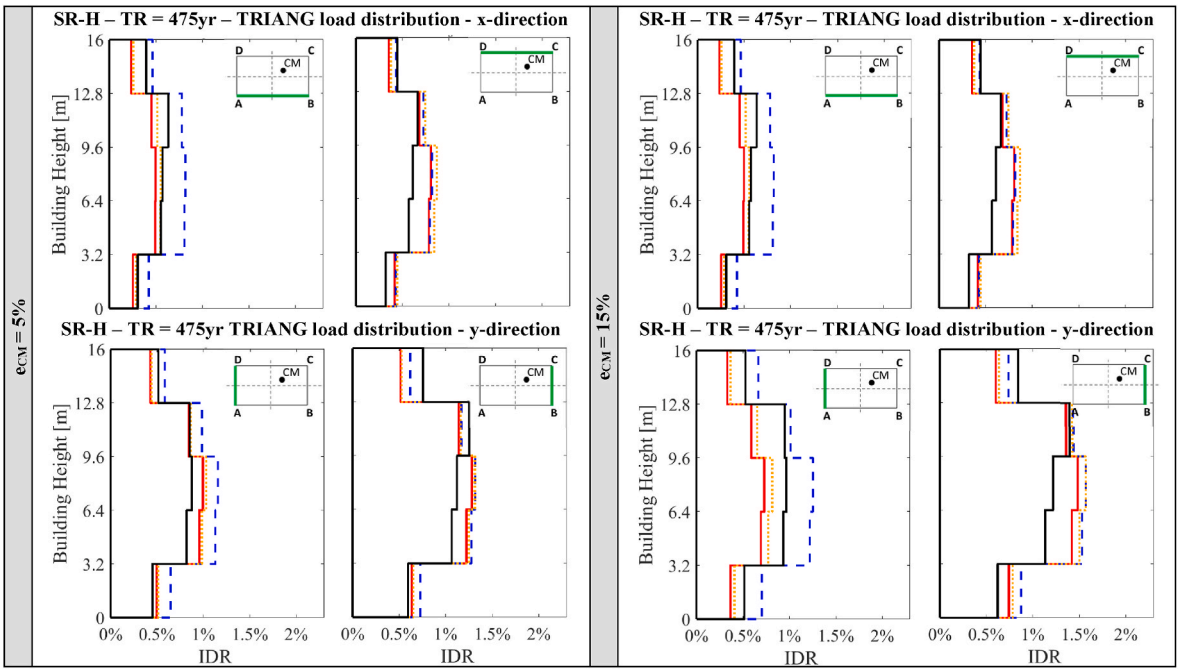

Fig. 16. SR-H building model: IDRs for e_{CM} = 5% (left) and e_{CM} = 15% (right) for T_R = 475years (TRIANG load pattern).

IDR observed.

If the IDRs of the two sides of the buildings provided by NTHAs are assumed as benchmark, the comparison between these IDRs and those determined by PO methods show the ability of these methods to capture the effects of the torsional component of the response on this EDP prediction. This comparison is in most case consistent with the conclusions reached for the RDR results. The N2 method appears to be inadequate in predicting the IDRs of the stiff sides (sides AB and AD) obtained by NTHAs. Indeed, the N2 method significantly and systematically underestimates the IDRs of the stiff sides. This underestimation is larger at the higher storeys where, however, the NTHAs return IDRs lower than the maximum value at the third storey. The application of the N2 method adjusted by the 100:30 combination rule has a negligible effect on the prediction of the IDRs (for both F and H models). Hence, it is confirmed than the 100:30 rule does not improve the prediction provided by the N2 method. On the other hand, the N2ext method leads to IDRs that are significantly closer to those obtained by NTHAs. In general (for both F and H buildings), the improvement achieved by the N2ext method is larger as the eccentricity increases.

Apparently, the IDRs of the stiff side of the GL-H and SR-H buildings obtained by NTHAs are well predicted by the N2 method in some cases and even overestimated in others (Figs. 14 and 16). However, this is the consequence of the overestimation of the CM displacement demand that also determines the overestimation of flexible side IDR. The N2 method is unconservative only for the stiff side of the SR-H building with large e_{CM} (Fig. 16). In these cases, the IDRs of the flexible side are well predicted, consistently with results obtained by the F model. The application of the N2ext method does not modify the prediction of the flexible side, while it increases the stiff side IDR. Hence, the N2ext method improves the prediction of the IDR in those cases where the N2 method is unconservative and is conservative in the other cases.

It should be noted that there are some differences between the results obtained by the H and F models both in the PO and in the NTHAs. Overall, the F models have smaller demands at the lower storeys and higher demands at the top two stories. The following factors contribute to the differences between the predictions of the two models: a) there are differences in the initial stiffness: in the F models the section follows the response of the concrete and steel fibres while in the H model the initial stiffness is taken as secant to 40% of the yield force, thus all columns are modelled as cracked at the start of the analysis. The corresponding PO curves are clearly affected by this assumption (see Fig. 3 and its discussion); b) the shapes of the IDR demands obtained from the PO and NTHAs are similar (for each model); c) there are differences in the nonlinear responses: the F models show greater torsional component than H models because the plastic hinge model (H) does not account for the M − N interaction.

To summarize the effects of the N2ext correction on the accuracy of the IDR demands by the N2 method Fig. 17 reports the third storey IDRs normalized with respect to the relevant CM IDRs. The third storey is selected since this is the storey that in most cases shows the largest IDR demands. The results are organized similarly to Fig. 11.

Fig. 17 shows that the N2ext method always improves the IDRs predicted by the N2 method with respect to the NTHAs since the deformed shape by the N2 method (which is represented by a straight line) is not able to capture the effects of the floor rotations on the IDR of the stiff side, and this aspect becomes more important for buildings with plan-irregularities. The N2ext enhances the prediction of in-plan distribution of the maximum IDR that assumes the typical V-shape, thus replicating that predicted by the NTHAs.

5. Summary and conclusions

This paper investigates the limitations of the N2 pushover analyses when applied to plan-asymmetric buildings and shows how in these cases the extended N2 method enhances the prediction of the nonlinear static analyses. Two five-storey case-study buildings representative of a large variety of old Italian structures built in the ‘70s, ‘80s and ‘90s are used to compare the predictions of the original N2 method with those of nonlinear time history analyses. The effects of the 100:30 directional combination and of the extended N2 method developed for plan irregular buildings are investigated. In order to check whether the effects are model-dependent, two different models are used for each building: one uses a beam-with-hinges continuum approach with a fibre-section discretization of the end hinges (F-model), the other one uses a lumped plasticity approach with end nonlinear springs with a moment-chord rotation relationship defined by a phenomenological law (H-model). The F-model accounts for the M_x-M_y-N interaction while the nonlinear springs of the H-model provide separate and independent relationships

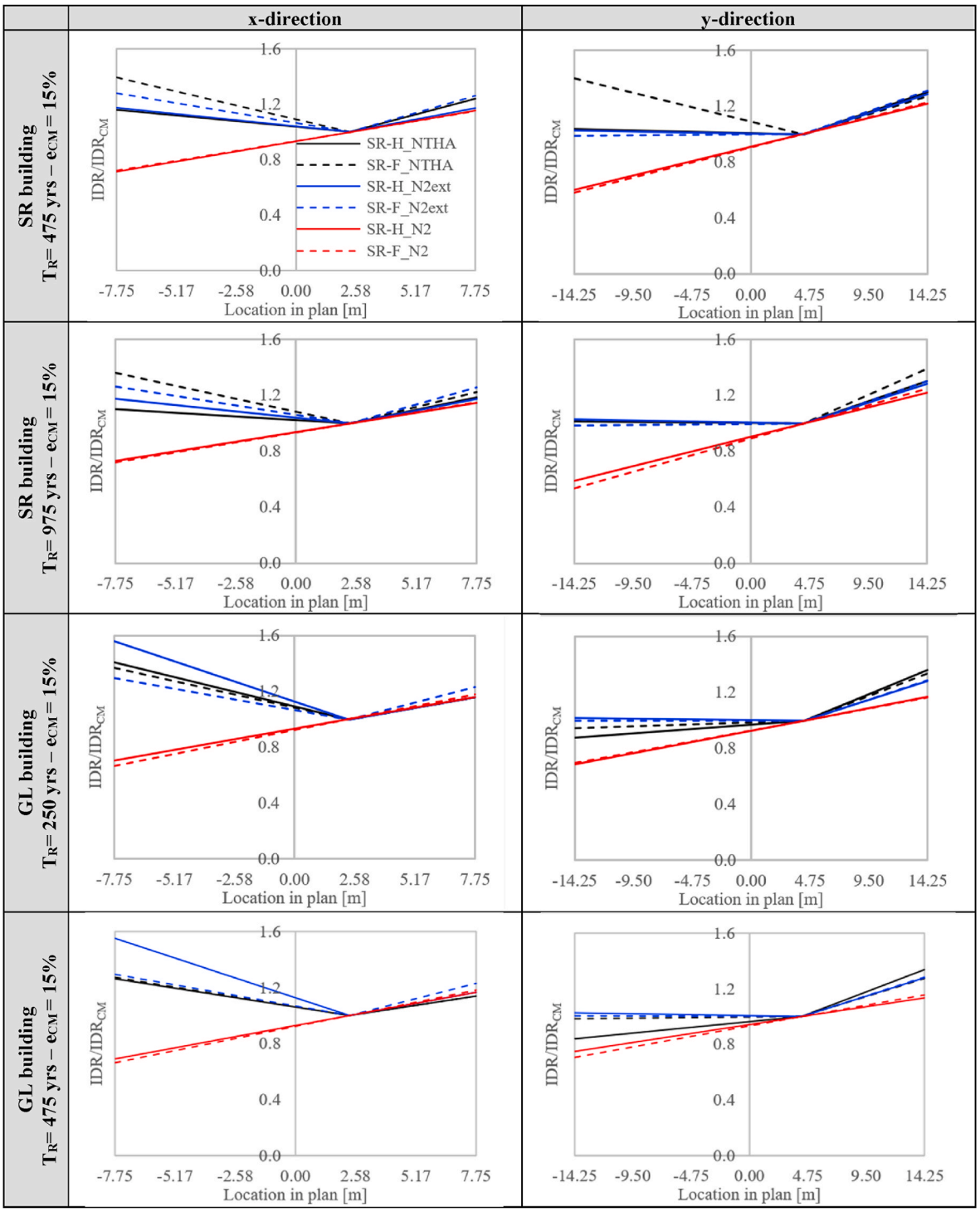

Fig. 17. Third floor IDRs normalized with respect to the CM IDR for SR building with T_R = 475 yrs (first row), SR building with T_R = 975 yrs (second row), the GL building with T_R = 250 yrs (third row) and the GL building with T_R = 475 yrs (fourth row). All cases refer to e_{CM} = 15%.

for the bending moments M_x and M_y, whose features are derived for a fixed axial load.

Different positions of the centre of mass (CM) are considered, more specifically low (5%) and large (15%) eccentricities between the CM and the plan geometric centre. Three different seismic hazard levels are considered for each building, more specifically, T_R = 50, 250 and 475 yrs for the GL building and T_R = 250, 475 and 975 yrs for the SR building. PO analyses were carried out using the N2 method (without and with the 100:30 directional combination rule) and the N2ext method. NTHAs, considered here as reference method of analysis, were carried out by applying a set of 20 pairs of recorded ground motions on each structure.

The main outcomes of the study are summarized hereafter:

a) The results obtained by NTH analyses show that the demand, in terms of both RDR and IDR, of the two sides of the buildings is generally larger than that of the centre of mass. This denotes an important torsional component of the response that amplifies the demand of the perimeter frames. This trend is shown in the x- and y-

directions in both case study buildings, for all return periods and for both F and H models. This effect is larger at the higher eccentricity.

b) The in-plan distribution of the demand predicted by the N2 method is linear and, due to the floor rotations, it is amplified at the flexible side with respect to the centre of mass. There is also a strong reduction in the prediction of the response of the stiff side that is in contrast to prediction from NTHAs. The inability of the N2 method to replicate all the effects of the torsional component of the response leads to systematically underestimate the response of the stiff side for both F and H models. The directional combination rule (100:30 in the present study, though similar results are expected from the SRSS rule) does not improve the prediction of seismic response of the N2 method.

c) The correction introduced by the N2ext method enhances the prediction of the in-plan distribution of the response in terms of RDR and IDR, particularly on the stiff side of plan asymmetric buildings. In most cases the N2ext demand shape replicates that of the NTH analyses. In general, for both F and H numerical models, the improvement in the prediction of torsional component of the seismic response achieved by the N2ext method becomes larger as the eccentricity increases.

d) The RDR and IDR of the PO and the NTH analyses may differ. The differences between PO and NTH analyses are mostly due to the approximations in the PO methods but also to the high variability of the results by NTHA's as a function of the ground motion selection process.

e) F and H models may provide different EDP demands both in the PO and in the NTH analyses. These differences are mainly due to: the initial stiffness of the two models; the greater influence of the floor rotations in the F model with respect to the H models, whose plastic hinges do not account for the M_x-M_y-N interaction; the different element hysteretic response of the two models.

f) When the response of the CM by PO analyses is not well predicted with respect to NTHAs, the N2ext method cannot enhance the response of the building perimeter frames. This happens for some H models: more specifically, for the lower eccentricity the N2ext method sometimes overestimates the response of the flexible sides with respect to NTHAs. However, this observation does not invalidate the use of the N2ext method for the prediction of the seismic response of plan asymmetric buildings. In fact, the results show that most of the deviations between the demand by NTHAs and by the N2ext method are due to the difference in the CM demand and not to incorrect assessment of the effect of the torsional component of the response.

g) In any case, the N2ext method, although sometimes is non-conservative compared to the NLTHA, generally improves the results produced by the NTHA.

Author statement

All authors of this research paper have directly participated in the planning, execution, or analysis of this study and writing of the manuscript.

Declaration of competing interest

The authors declare that they have no known competing financial interests or personal relationships that could have appeared to influence the work reported in this paper.

Data availability

Data will be made available on request.

Acknowledgements

The study presented in this article was developed within the activities of WP11 of the ReLUIS-DPC 2019–2021 research program funded by the Italian Civil Protection Agency (DPC). The opinions and conclusions presented by the authors do not necessarily reflect those of the funding agency.

Appendix. 6

6.1 Cross sections and reinforcement data of the case study buildings

Table A.1
GL building column cross sections (width x depth, in cm) at different storeys

Storey	Column							
	1, 8, 25, 32	2, 7,26, 31	3, 6, 27, 30	4, 5, 28, 29	9, 16, 17, 24	10, 15, 18, 23	11, 14, 19, 22	12, 13, 20, 21
5	30x40	30x40	30x40	30x40	30x40	30x40	30x40	30x40
4	30x40	30x40	30x40	30x40	30x40	30x40	30x40	30x40
3	30x40	30x40	30x40	30x40	30x40	30x50	30x50	30x40
2	30x40	30x40	30x40	30x40	30x40	30x60	30x60	30x50
1	30x40	30x50	30x50	30x40	30x50	30x70	30x70	30x60

Table A.2
SR building column cross sections (width x depth, in cm) at different storeys

Storey	Column							
	1, 8, 25, 32	2, 7,26, 31	3, 6, 27, 30	4, 5, 28, 29	9, 16, 17, 24	10, 15, 18, 23	11, 14, 19, 22	12, 13, 20, 21
5	30x40	30x40	30x40	30x40	30x40	30x50	30x50	30x50
4	30x40	30x40	30x40	30x40	30x50	30x50	30x50	30x50
3	30x40	30x50	30x50	30x50	30x50	40x50	40x50	40x50
2	30x50	40x50	40x50	40x50	30x50	40x60	40x60	40x60
1	30x50	40x60	40x60	40x60	30x60	40x70	40x70	40x70

Table A.3
GL Building: Reinforcements of the columns

Column	First Floor	Second Floor	Third Floor	Fourth Floor	Fifth Floor
1-8-25-32	6φ14	6φ14	6φ14	6φ14	6φ14
2-3-6-7-26-27-30-31	8φ14	6φ14	6φ14	6φ14	6φ14
4-5-28-29	8φ14	6φ14	6φ14	6φ14	6φ14
9-16-17-24	8φ14	6φ14	6φ14	6φ14	6φ14
10-11-14-15-18-19-22-23	10φ14	8φ14	6φ14	6φ14	6φ14
12-13-20-21	10φ14	8φ14	6φ14	6φ14	6φ14

Table A.4
SR Building: Reinforcements of the columns

Column	First Floor	Second Floor	Third Floor	Fourth Floor	Fifth Floor
1-8-25-32	8φ14+2φ20	8φ14+2φ20	12φ14	10φ14	10φ14
2-3-6-7-26-27-30-31	6φ14 + 14φ20	10φ14	6φ14+4φ20	8φ14+6φ20	10φ14
4-5-28-29	6φ14 + 14φ20	12φ14	8φ14+4φ20	2φ14 + 10φ20	6φ14+4φ20
9-16-17-24	10φ20+6φ14	8φ20+2φ14	6φ20+2φ14	8φ14+2φ20	10φ14
10-11-14-15-18-19-22-23	8φ14 + 22φ20	6φ14+6φ20	6φ14+8φ20	6φ14 + 10φ20	10φ14
12-13-20-21	8φ14 + 20φ20	6φ14+6φ20	6φ14+8φ20	6φ14 + 10φ20	10φ14

Table A.5
GL building. Reinforcement of the beams (the beams have equal 30 × 60 cm cross sections and reinforcement at all floors).

Frame	Pos.	1	2	2	3	3	4	4	5	5	6	6	7	7	8
		25	26	26	27	27	28	28	29	29	30	30	31	31	32
X1-X4	Top	2φ14	4φ14	4φ14	3φ14	3φ14	3φ14	3φ14	3φ14	3φ14	3φ14	3φ14	4φ14	4φ14	2φ14
	Bottom	3φ14	3φ14	2φ14	2φ14	2φ14	2φ14	2φ14	2φ14	2φ14	2φ14	2φ14	2φ14	3φ14	3φ14
	Sides (both)	4φ14	4φ14	4φ14	4φ14	4φ14	4φ14	4φ14	4φ14	4φ14	4φ14	4φ14	4φ14	4φ14	4φ14

Frame	Pos.	9	10	10	11	11	12	12	13	13	14	14	15	15	16
		17	18	18	19	19	20	20	21	21	22	22	23	23	24
X2-X3	Top	3φ14	2φ20+2φ14	2φ20+2φ14	5φ14	5φ14	4φ14	4φ14	4φ14	4φ14	5φ14	5φ14	2φ20+2φ14	2φ20+2φ14	3φ14
	Bottom	4φ14	4φ14	3φ14	3φ14	3φ14	3φ14	2φ14	2φ14	3φ14	3φ14	3φ14	3φ14	4φ14	4φ14
	Sides (both)	4φ14	4φ14	4φ14	4φ14	4φ14	4φ14	4φ14	4φ14	4φ14	4φ14	4φ14	4φ14	4φ14	4φ14

Frame	Pos.	1	9	9	17	17	25
		8	16	16	24	24	32
Y1–Y8	Top	2φ14	3φ14	3φ14	3φ14	3φ14	2φ14
	Bottom	2φ14	2φ14	2φ14	2φ14	2φ14	2φ14
	Sides (both)	4φ14	4φ14	4φ14	4φ14	4φ14	4φ14

Table A.6
SR building: Reinforcement details of the beams.

Frame	Level	Pos.	1	2	2	3	3	4	4	5	5	6	6	7	7	8
			25	26	26	27	27	28	28	29	29	30	30	31	31	32
X1-X4 (30x60)	1–2	Top	2φ20	3φ20+ 1φ14	3φ20+ 1φ14	3φ20+ 1φ14	3φ20+ 1φ14	3φ20	3φ20	3φ20	3φ20	3φ20+ 1φ14	3φ20+1φ14	3φ20+ 1φ14	3φ20+ 1φ14	2φ20
		Bottom	4φ14	2φ20	2φ20	2φ20	2φ20	2φ20	2φ20	2φ20	2φ20	2φ20	2φ20	2φ20	2φ20	4φ14
		Sides	2φ14	2φ14	2φ14	2φ14	2φ14	2φ14	2φ14	2φ14	2φ14	2φ14	2φ14	2φ14	2φ14	2φ14
	3	Top	2φ20	3φ20	3φ20	3φ20	3φ20	3φ20	3φ20	3φ20	3φ20	3φ20	3φ20	3φ20	3φ20	2φ20
		Bottom	4φ14	2φ20	2φ20	2φ20	2φ20	2φ20	2φ20	2φ20	2φ20	2φ20	2φ20	2φ20	2φ20	4φ14
		Sides	2φ14	2φ14	2φ14	2φ14	2φ14	2φ14	2φ14	2φ14	2φ14	2φ14	2φ14	2φ14	2φ14	2φ14
	4	Top	2φ20	2φ20+ 1φ14	2φ20+ 1φ14	2φ20+ 1φ14	2φ20+ 1φ14	2φ20	2φ20	2φ20	2φ20	2φ20+ 1φ14	2φ20+ 1φ14	2φ20+ 1φ14	2φ20+ 1φ14	2φ20
		Bottom	4φ14	4φ14	4φ14	4φ14	4φ14	4φ14	4φ14	4φ14	4φ14	4φ14	4φ14	4φ14	4φ14	4φ14
		Sides	2φ14	2φ14	2φ14	2φ14	2φ14	2φ14	2φ14	2φ14	2φ14	2φ14	2φ14	2φ14	2φ14	2φ14
	5	Top	3φ14	2φ20	2φ20	2φ20	2φ20	3φ14	3φ14	3φ14	3φ14	2φ20	2φ20	2φ20	2φ20	3φ14
		Bottom	3φ14	4φ14	4φ14	4φ14	4φ14	3φ14	3φ14	3φ14	3φ14	4φ14	4φ14	4φ14	4φ14	3φ14
		Sides	2φ14	2φ14	2φ14	2φ14	2φ14	2φ14	2φ14	2φ14	2φ14	2φ14	2φ14	2φ14	2φ14	2φ14

Frame	Level	Pos.	9	10	10	11	11	12	12	13	13	14	14	15	15	16
			17	18	18	19	19	20	20	21	21	22	22	23	23	24
X2-X3 (30x60)	1	Top	2φ20	4φ20	4φ20	4φ20	4φ20	3φ20+ 1φ14	3φ20+ 1φ14	3φ20+ 1φ14	3φ20+1φ14	4φ20	4φ20	4φ20	4φ20	2φ20
		Bottom	4φ14	2φ20	2φ20	2φ20	2φ20	2φ20	2φ20	2φ20	2φ20	2φ20	2φ20	2φ20	2φ20	4φ14
		Sides	2φ14	2φ14	2φ14	2φ14	2φ14	2φ14	2φ14	2φ14	2φ14	2φ14	2φ14	2φ14	2φ14	2φ14
	2	Top	2φ20+ 1φ14	4φ20	4φ20	4φ20	4φ20	3φ20+ 1φ14	3φ20+ 1φ14	3φ20+ 1φ14	3φ20+1φ14	4φ20	4φ20	4φ20	4φ20	2φ20+ 1φ14
		Bottom	4φ14	2φ20	2φ20	2φ20	2φ20	2φ20	2φ20	2φ20	2φ20	2φ20	2φ20	2φ20	2φ20	4φ14
		Sides	2φ14	2φ14	2φ14	2φ14	2φ14	2φ14	2φ14	2φ14	2φ14	2φ14	2φ14	2φ14	2φ14	2φ14
	3	Top	2φ20	4φ20	4φ20	3φ20+ 1φ14	3φ20+ 1φ14	3φ20+ 1φ14	3φ20+ 1φ14	3φ20+ 1φ14	3φ20+ 1φ14	3φ20+ 1φ14	3φ20+ 1φ14	4φ20	4φ20	2φ20
		Bottom	4φ14	2φ20	2φ20	2φ20	2φ20	2φ20	2φ20	2φ20	2φ20	2φ20	2φ20	2φ20	2φ20	4φ14
		Sides	2φ14	2φ14	2φ14	2φ14	2φ14	2φ14	2φ14	2φ14	2φ14	2φ14	2φ14	2φ14	2φ14	2φ14
	4	Top	2φ20	3φ20+ 1φ14	3φ20+ 1φ14	3φ20	3φ20	2φ20+ 1φ14	2φ20+ 1φ14	2φ20+ 1φ14	2φ20+ 1φ14	3φ20	3φ20	3φ20+ 1φ14	3φ20+ 1φ14	2φ20
		Bottom	4φ14	2φ20	2φ20	2φ20	2φ20	4φ14	4φ14	4φ14	4φ14	2φ20	2φ20	2φ20	2φ20	4φ14
		Sides	2φ14	2φ14	2φ14	2φ14	2φ14	2φ14	2φ14	2φ14	2φ14	2φ14	2φ14	2φ14	2φ14	2φ14
	5	Top	3φ14	3φ20	3φ20	2φ20+ 1φ14	2φ20+ 1φ14	2φ20	2φ20	2φ20	2φ20	2φ20+ 1φ14	2φ20+ 1φ14	3φ20	3φ20	3φ14
		Bottom	3φ14	2φ20	2φ20	4φ14	4φ14	4φ14	4φ14	4φ14	4φ14	4φ14	4φ14	2φ20	2φ20	3φ14
		Sides	2φ14	2φ14	2φ14	2φ14	2φ14	2φ14	2φ14	2φ14	2φ14	2φ14	2φ14	2φ14	2φ14	2φ14

Frame	Level	Pos.	1	9	9	17	17	25	Frame	Level	2	10	10	18	18	26
			8	16	16	24	24	32			7	15	15	23	23	31
Y1–Y8 (30x60)	1	Top	3φ20	3φ20+ 1φ14	3φ20+ 1φ14	3φ20+ 1φ14	3φ20+ 1φ14	3φ20	Y2–Y7 (80x24)	1	6φ20	6φ20+ 1φ14	6φ20+ 1φ14	6φ20+ 1φ14	6φ20+ 1φ14	6φ20
		Bottom	2φ20	2φ20	2φ20	2φ20	2φ20	2φ20			4φ20	4φ20	4φ20	4φ20	4φ20	4φ20
		Sides	2φ14	2φ14	2φ14	2φ14	2φ14	2φ14			–	–	–	–	–	–
	2	Top	3φ20	3φ20+ 1φ14	3φ20+ 1φ14	3φ20+ 1φ14	3φ20+ 1φ14	3φ20		2	7φ20	7φ20+ 1φ14	7φ20+ 1φ14	7φ20+ 1φ14	7φ20+ 1φ14	7φ20
		Bottom	2φ20	2φ20	2φ20	2φ20	2φ20	2φ20			4φ20+ 1φ14	4φ20+ 1φ14	4φ20+ 1φ14	4φ20+ 1φ14	4φ20+ 1φ14	4φ20+ 1φ14
		Sides	2φ14	2φ14	2φ14	2φ14	2φ14	2φ14			–	–	–	–	–	–
	3	Top	3φ20	3φ20	3φ20	3φ20	3φ20	3φ20		3	6φ20+ 1φ14	7φ20	7φ20	7φ20	7φ20	6φ20+ 1φ14
		Bottom	3φ14	2φ20	2φ20	2φ20	2φ20	3φ14			4φ20	4φ20	4φ20	4φ20	4φ20	4φ20

(*continued on next page*)

Table A.6 (*continued*)

Frame	Level	Pos.	1	9	9	17	17	25	Frame	Level	2	10	10	18	18	26
			8	16	16	24	24	32			7	15	15	23	23	31
		Sides	2φ14	2φ14	2φ14	2φ14	2φ14	2φ14			–	–	–	–	–	–
	4	Top	2φ20	3φ20	3φ20	3φ20	3φ20	2φ20		4	5φ20	5φ20	5φ20	5φ20	5φ20	5φ20
		Bottom	4φ14	3φ14	3φ14	3φ14	3φ14	4φ14			6φ14	6φ14	6φ14	6φ14	6φ14	6φ14
		Sides	2φ14	2φ14	2φ14	2φ14	2φ14	2φ14			–	–	–	–	–	–
	5	Top	3φ14	3φ14	3φ14	3φ14	3φ14	3φ14		5	3φ20+ 1φ14	3φ20+ 1φ14	3φ20+ 1φ14	3φ20+ 1φ14	3φ20+ 1φ14	3φ20+ 1φ14
		Bottom	3φ14	3φ14	3φ14	3φ14	3φ14	3φ14			4φ14	4φ14	4φ14	4φ14	4φ14	4φ14
		Sides	2φ14	2φ14	2φ14	2φ14	2φ14	2φ14			–	–	–	–	–	–
Frame	Level	Pos.	3	11	11	19	19	27	Frame	Level	4	12	12	20	20	28
			6	14	14	22	22	30			5	13	13	21	21	29
Y3–Y6 (80x24)	1	Top	6φ20	6φ20+ 1φ14	6φ20+ 1φ14	6φ20+ 1φ14	6φ20+1φ14	6φ20	Y4–Y5 (80x24)	1	6φ20+ 1φ14	6φ20+ 1φ14	6φ20+ 1φ14	6φ20+ 1φ14	6φ20+ 1φ14	6φ20+ 1φ14
		Bottom	4φ20	4φ20	4φ20	4φ20	4φ20	4φ20			3φ20+ 1φ14	3φ20+ 1φ14	3φ20+ 1φ14	3φ20+ 1φ14	3φ20+ 1φ14	3φ20+ 1φ14
		Sides	–	–	–	–	–	–			–	–	–	–	–	–
	2	Top	7φ20	7φ20+ 1φ14	7φ20+ 1φ14	7φ20+ 1φ14	7φ20+1φ14	7φ20		2	7φ20+ 1φ14	7φ20+ 1φ14	7φ20+ 1φ14	7φ20+ 1φ14	7φ20+ 1φ14	7φ20+ 1φ14
		Bottom	4φ20+ 1φ14	4φ20+ 1φ14	4φ20+ 1φ14	4φ20+ 1φ14	4φ20+1φ14	4φ20+ 1φ14			4φ20+ 1φ14	4φ20+ 1φ14	4φ20+ 1φ14	4φ20+ 1φ14	4φ20+ 1φ14	4φ20+ 1φ14
		Sides	–	–	–	–	–	–			–	–	–	–	–	–
	3	Top	6φ20+ 1φ14	7φ20	7φ20	7φ20	280245	6φ20+ 1φ14		3	6φ20+ 1φ14	7φ20	7φ20	7φ20	7φ20	6φ20+ 1φ14
		Bottom	4φ20	4φ20	4φ20	4φ20		4φ20			4φ20	4φ20	4φ20	4φ20	4φ20	4φ20
		Sides	–	–	–	–		–			–	–	–	–	–	–
	4	Top	5φ20	5φ20	5φ20	5φ20	5φ20	5φ20		4	5φ20	5φ20+ 1φ14	5φ20+ 1φ14	5φ20+ 1φ14	5φ20+ 1φ14	5φ20
		Bottom	6φ14	6φ14	6φ14	6φ14	6φ14	6φ14			6φ14	6φ14	6φ14	6φ14	6φ14	6φ14
		Sides	–	–	–	–	–	–			–	–	–	–	–	–
	5	Top	3φ20+ 1φ14	3φ20+ 1φ14	3φ20+ 1φ14	3φ20+ 1φ14	3φ20+1φ14	3φ20+ 1φ14		5	6φ14	4φ20	4φ20	4φ20	4φ20	6φ14
		Bottom	4φ14	4φ14	4φ14	4φ14	4φ14	4φ14			4φ14	4φ14	4φ14	4φ14	4φ14	4φ14
		Sides	–	–	–	–	–	–			–	–	–	–	–	–

6.2 Data of the selected ground motion records

Table A.7
Ground motion records selected for $T_R = 50$ years and used for the NTHAs of the GL-F and GL-H buildings

n.	Database	Station ID	Earthquake Name	Date	Time (UTC)	Mw	Epicentral Distance (km)	Site class	Scale Factor
1	ESD	ATH4	Greece	07/09/1999	11:56:49	5.9	19.7	A	1.38440
2	ESD	CLO	Central Italy	26/10/2016	19:18:06	5.9	10.8	A	2.39796
3	ESD	MNF	Central Italy	26/10/2016	19:18:06	5.9	17.4	A	1.72020
4	ESD	ST26	Friuli (aftershock)	15/09/1976	09:21:19	6	12	A	0.98348
5	ESD	ST136	Umbria	29/04/1984	05:02:59	5.6	17	A	4.61176
6	ESD	ST26	Friuli (aftershock)	11/09/1976	16:31:11	5.3	8	A	0.51628
7	ESD	ST266	Umbria Marche (aftershock)	14/10/1997	15:23:00	5.6	12	A	3.77873
8	ESD	ST234	Umbria Marche (aftershock)	21/03/1998	16:45:10	5	14	A	2.85256
9	ESD	ST2487	South Iceland	17/06/2000	15:40:41	6.5	13	A	2.86853
10	ESD	ST2496	Mt. Hengill Area	04/06/1998	21:36:54	5.4	18	A	1.78594
11	ESD	ST2497	Mt. Hengill Area	04/06/1998	21:36:54	5.4	15	A	1.23087
12	ESD	ST2556	Mt. Hengill Area	04/06/1998	21:36:54	5.4	15	A	0.43376
13	ESD	ST2950	NE of Banja Luka	13/08/1981	02:58:12	5.7	10	A	0.15003
14	ESD	ST1320	Kozani	13/05/1995	08:47:15	6.5	17	A	0.43781
15	ESD	ST2496	South Iceland (aftershock)	21/06/2000	00:51:48	6.4	14	A	0.32210
16	ESD	ST2483	South Iceland (aftershock)	21/06/2000	00:51:48	6.4	6	A	0.30825
17	ESD	ST2557	South Iceland (aftershock)	21/06/2000	00:51:48	6.4	15	A	0.23434
18	ESM	ST2497	South Iceland (aftershock)	21/06/2000	00:51:48	6.4	20	A	1.18337
19	ESM	ST2556	South Iceland (aftershock)	21/06/2000	00:51:48	6.4	20	A	0.84804
20	ESM	ST539	Bingol	01/05/2003	00:27:04	6.3	14	A	0.83311

Table A.8
Ground motion records selected for $T_R = 250$ years and used for the NTHAs of the GL-F and GL-H buildings

n.	Database	Station ID	Earthquake Name	Date	Time (UTC)	Mw	Epicentral Distance (km)	Site class	Scale Factor
1	ESD	ST26	Friuli (aftershock)	15/09/1976	09:21:19	6	12	A	3.42232
2	ESD	ST61	Valnerina	19/09/1979	21:35:37	5.8	22	A	4.41300
3	ESD	ST93	Campano Lucano	23/11/1980	18:34:52	6.9	23	A	0.50460
4	ESD	ST100	Campano Lucano	23/11/1980	18:34:52	6.9	26	A	0.64607
5	ESD	ST161	Golbasi	05/05/1986	03:35:38	6	29	A	2.70732
6	ESD	ST1320	Kozani	13/05/1995	08:47:15	6.5	17	A	3.07186
7	ESD	ST2494	South Iceland	17/06/2000	15:40:41	6.5	29	A	3.43004
8	ESD	ST2496	South Iceland (aftershock)	21/06/2000	00:51:48	6.4	14	A	1.08252
9	ESD	ST2552	South Iceland (aftershock)	21/06/2000	00:51:48	6.4	24	A	1.60418
10	ESD	ST2557	South Iceland (aftershock)	21/06/2000	00:51:48	6.4	15	A	1.09263
11	ESD	ST2563	South Iceland (aftershock)	21/06/2000	00:51:48	6.4	24	A	1.79065
12	ESD	ST2497	South Iceland (aftershock)	21/06/2000	00:51:48	6.4	20	A	0.80385
13	ESD	ST2556	South Iceland (aftershock)	21/06/2000	00:51:48	6.4	20	A	0.76930
14	ESD	ST539	Bingol	01/05/2003	00:27:04	6.3	14	A	0.58484
15	ESM	ULA	Northwestern Balkan Peninsula	15/04/1979	06:19:41	6.9	19.7	A	0.56934
16	ESM	ATH4	Greece	07/09/1999	11:56:49	5.9	19.7	A	2.95331
17	ESM	CLO	Central Italy	26/10/2016	19:18:06	5.9	10.8	A	2.11643
18	ESM	MMO	Central Italy	26/10/2016	19:18:06	5.9	16.2	A	2.67104
19	ESM	MNF	Central Italy	26/10/2016	19:18:06	5.9	17.4	A	2.07916
20	ESM	T1213	Central Italy	30/10/2016	06:40:18	6.5	12	A	0.54824

Table A.9
Ground motion records selected for $T_R = 475$ years and used for the NTHAs of the GL-F and GL-H buildings

n.	Database	Station ID	Earthquake Name	Date	Time (UTC)	Mw	Epicentral Distance (km)	Site class	Scale Factor
1	ESD	ST20	Friuli	06/05/1976	20:00:13	6.5	23	A	1.93614
2	ESD	ST98	Campano Lucano	23/11/1980	18:34:52	6.9	25	A	3.44217
3	ESD	ST100	Campano Lucano	23/11/1980	18:34:52	6.9	26	A	0.88546
4	ESD	ST2486	South Iceland	17/06/2000	15:40:41	6.5	5	A	0.46930
5	ESD	ST2487	South Iceland	17/06/2000	15:40:41	6.5	13	A	1.76590
6	ESD	ST2494	South Iceland	17/06/2000	15:40:41	6.5	29	A	4.70098
7	ESD	ST2496	South Iceland (aftershock)	21/06/2000	00:51:48	6.4	14	A	1.48363
8	ESD	ST2483	South Iceland (aftershock)	21/06/2000	00:51:48	6.4	6	A	0.51318
9	ESD	ST2487	South Iceland (aftershock)	21/06/2000	00:51:48	6.4	28	A	3.31828
10	ESD	ST2557	South Iceland (aftershock)	21/06/2000	00:51:48	6.4	15	A	1.49748
11	ESD	ST2563	South Iceland (aftershock)	21/06/2000	00:51:48	6.4	24	A	2.45414
12	ESD	ST2497	South Iceland (aftershock)	21/06/2000	00:51:48	6.4	20	A	1.10170
13	ESD	ST2556	South Iceland (aftershock)	21/06/2000	00:51:48	6.4	20	A	1.05435
14	ESD	ST2558	South Iceland (aftershock)	21/06/2000	00:51:48	6.4	5	A	0.53032
15	ESD	ST539	Bingol	01/05/2003	00:27:04	6.3	14	A	0.80155
16	ESM	ULA	Northwestern Balkan Peninsula	15/04/1979	06:19:41	6.9	19.7	A	0.78030

(*continued on next page*)

Table A.9 (*continued*)

n.	Database	Station ID	Earthquake Name	Date	Time (UTC)	Mw	Epicentral Distance (km)	Site class	Scale Factor
17	ESM	ATH4	Greece	07/09/1999	11:56:49	5.9	19.7	A	4.04762
18	ESM	CLO	Central Italy	30/10/2016	06:40:18	6.5	7.8	A	0.52078
19	ESM	MMO	Central Italy	26/10/2016	19:18:06	5.9	16.2	A	3.66076
20	ESM	MNF	Central Italy	26/10/2016	19:18:06	5.9	17.4	A	2.84956

Table A.10
Ground motion records selected for $T_R = 250$ years and used for the NTHAs of the SR-F building

n.	Database	Station ID	Earthquake Name	Date	Time (UTC)	Mw	Epicentral Distance (km)	Site class	Scale Factor
1	ESD	ST225	Valnerina	19/09/1979	21:35:37	5.8	5	A	2.36521
2	ESD	ST98	Campano Lucano	23/11/1980	18:34:52	6.9	25	A	2.16568
3	ESD	ST143	Lazio Abruzzo	07/05/1984	17:49:42	5.9	22	A	3.89385
4	ESD	ST2487	South Iceland	17/06/2000	15:40:41	6.5	13	A	1.69629
5	ESD	ST1320	Kozani	13/05/1995	08:47:15	6.5	17	A	2.47838
6	ESD	ST2496	South Iceland (aftershock)	21/06/2000	00:51:48	6.4	14	A	1.06063
7	ESD	ST2552	South Iceland (aftershock)	21/06/2000	00:51:48	6.4	24	A	2.89584
8	ESD	ST2486	South Iceland (aftershock)	21/06/2000	00:51:48	6.4	22	A	2.38927
9	ESD	ST2487	South Iceland (aftershock)	21/06/2000	00:51:48	6.4	28	A	4.36148
10	ESD	ST2557	South Iceland (aftershock)	21/06/2000	00:51:48	6.4	15	A	1.25725
11	ESD	ST2563	South Iceland (aftershock)	21/06/2000	00:51:48	6.4	24	A	2.66681
12	ESD	ST2556	South Iceland (aftershock)	21/06/2000	00:51:48	6.4	20	A	1.39983
13	ESM	ST539	Bingol	01/05/2003	00:27:04	6.3	14	A	0.76187
14	ESM	MZ14	Central Italy	30/10/2016	06:40:18	6.5	30.6	A	1.91158
15	ESM	MZ19	Central Italy	30/10/2016	06:40:18	6.5	22.6	A	0.47612
16	ESM	ULA	Northwestern Balkan Peninsula	15/04/1979	06:19:41	6.9	19.7	A	0.54061
17	ESM	ATH4	Greece	07/09/1999	11:56:49	5.9	19.7	A	2.51900
18	ESM	CLO	Central Italy	26/10/2016	19:18:06	5.9	10.8	A	1.09382
19	ESM	MMO	Central Italy	26/10/2016	19:18:06	5.9	16.2	A	1.64306
20	ESM	MNF	Central Italy	26/10/2016	19:18:06	5.9	17.4	A	2.10188

Table A.11
Ground motion records selected for $T_R = 475$ years and used for the NTHAs of the SR-F building

n.	Database	Station ID	Earthquake Name	Date	Time (UTC)	Mw	Epicentral Distance (km)	Site class	Scale Factor
1	ESD	ST20	Friuli	06/05/1976	20:00:13	6.5	23	A	1.23690
2	ESD	ST54	Tabas	16/09/1978	15:35:57	7.3	12	A	0.87883
3	ESD	ST100	Campano Lucano	23/11/1980	18:34:52	6.9	26	A	1.09586
4	ESD	ST161	Golbasi	05/05/1986	03:35:38	6	29	A	4.00584
5	ESD	ST2486	South Iceland	17/06/2000	15:40:41	6.5	5	A	0.42793
6	ESD	ST1320	Kozani	13/05/1995	08:47:15	6.5	17	A	3.39670
7	ESD	ST2496	South Iceland (aftershock)	21/06/2000	00:51:48	6.4	14	A	1.45363
8	ESD	ST2552	South Iceland (aftershock)	21/06/2000	00:51:48	6.4	24	A	3.96885
9	ESD	ST2557	South Iceland (aftershock)	21/06/2000	00:51:48	6.4	15	A	1.72310
10	ESD	ST2563	South Iceland (aftershock)	21/06/2000	00:51:48	6.4	24	A	3.65495
11	ESD	ST2497	South Iceland (aftershock)	21/06/2000	00:51:48	6.4	20	A	2.17083
12	ESD	ST539	Bingol	01/05/2003	00:27:04	6.3	14	A	1.04417
13	ESM	MZ14	Central Italy	30/10/2016	06:40:18	6.5	30.6	A	2.61989
14	ESM	MZ19	Central Italy	30/10/2016	06:40:18	6.5	22.6	A	0.65253
15	ESM	ULA	Northwestern Balkan Peninsula	15/04/1979	06:19:41	6.9	19.7	A	0.74093
16	ESM	ATH4	Greece	07/09/1999	11:56:49	5.9	19.7	A	3.45238
17	ESM	CLO	Central Italy	26/10/2016	19:18:06	5.9	10.8	A	1.49912
18	ESM	CLO	Central Italy	30/10/2016	06:40:18	6.5	7.8	A	0.36180
19	ESM	MMO	Central Italy	26/10/2016	19:18:06	5.9	16.2	A	2.25187
20	ESM	T1213	Central Italy	30/10/2016	06:40:18	6.5	12	A	0.57789

Table A.12
Ground motion records selected for $T_R = 975$ years and used for the NTHAs of the SR-F building

n.	Database	Station ID	Earthquake Name	Date	Time (UTC)	Mw	Epicentral Distance (km)	Site class	Scale Factor
1	ESD	ST20	Friuli	06/05/1976	20:00:13	6.5	23	A	1.6903
2	ESD	ST54	Tabas	16/09/1978	15:35:57	7.3	12	A	1.2010
3	ESD	ST225	Valnerina	19/09/1979	21:35:37	5.8	5	A	4.4298
4	ESD	ST96	Campano Lucano	23/11/1980	18:34:52	6.9	32	A	0.6132
5	ESD	ST98	Campano Lucano	23/11/1980	18:34:52	6.9	25	A	4.0561
6	ESD	ST561	Izmit	17/08/1999	00:01:40	7.6	47	A	1.6044
7	ESD	ST575	Izmit	17/08/1999	00:01:40	7.6	9	A	0.9505

(*continued on next page*)

Table A.12 (*continued*)

n.	Database	Station ID	Earthquake Name	Date	Time (UTC)	Mw	Epicentral Distance (km)	Site class	Scale Factor
8	ESD	ST2486	South Iceland	17/06/2000	15:40:41	6.5	5	A	0.5848
9	ESD	ST2487	South Iceland	17/06/2000	15:40:41	6.5	13	A	3.1770
10	ESD	ST2496	South Iceland (aftershock)	21/06/2000	00:51:48	6.4	14	A	1.9864
11	ESD	ST2557	South Iceland (aftershock)	21/06/2000	00:51:48	6.4	15	A	2.3547
12	ESD	ST2563	South Iceland (aftershock)	21/06/2000	00:51:48	6.4	24	A	4.9946
13	ESD	ST2497	South Iceland (aftershock)	21/06/2000	00:51:48	6.4	20	A	2.9665
14	ESD	ST2558	South Iceland (aftershock)	21/06/2000	00:51:48	6.4	5	A	0.6554
15	ESD	ST539	Bingol	01/05/2003	00:27:04	6.3	14	A	1.4269
16	ESM	ATH4	Greece	07/09/1999	11:56:49	5.9	19.7	A	4.7178
17	ESM	ACC	Central Italy	30/10/2016	06:40:18	6.5	18.6	A	0.5980
18	ESM	MMO	Central Italy	26/10/2016	19:18:06	5.9	16.2	A	3.0773
19	ESM	T1213	Central Italy	30/10/2016	06:40:18	6.5	12	A	0.7897
20	ESM	4101	Izmit	17/08/1999	00:01:38	7.6	3.4	A	0.9255

Table A.13
Ground motion records selected for $T_R = 250$ years and used for the NTHAs of the SR-H building

n.	Database	Station ID	Earthquake Name	Date	Time (UTC)	Mw	Epicentral Distance (km)	Site class	Scale Factor
1	ESD	ST54	Tabas	16/09/1978	15:35:57	7.3	12	A	0.5567
2	ESD	ST225	Valnerina	19/09/1979	21:35:37	5.8	5	A	2.7696
3	ESD	ST98	Campano Lucano	23/11/1980	18:34:52	6.9	25	A	2.2302
4	ESD	ST100	Campano Lucano	23/11/1980	18:34:52	6.9	26	A	0.6327
5	ESD	ST143	Lazio Abruzzo	07/05/1984	17:49:42	5.9	22	A	3.7011
6	ESD	ST2556	Mt. Hengill Area	04/06/1998	21:36:54	5.4	15	A	4.7109
7	ESD	ST2558	South Iceland	17/06/2000	15:40:41	6.5	15	A	1.2362
8	ESD	ST2496	South Iceland (aftershock)	21/06/2000	00:51:48	6.4	14	A	0.9559
9	ESD	ST2486	South Iceland (aftershock)	21/06/2000	00:51:48	6.4	22	A	2.3674
10	ESD	ST2557	South Iceland (aftershock)	21/06/2000	00:51:48	6.4	15	A	0.9924
11	ESD	ST2563	South Iceland (aftershock)	21/06/2000	00:51:48	6.4	24	A	2.4075
12	ESD	ST2497	South Iceland (aftershock)	21/06/2000	00:51:48	6.4	20	A	1.4749
13	ESD	ST539	Bingol	01/05/2003	00:27:04	6.3	14	A	0.6511
14	ESM	MZ11	Central Italy	30/10/2016	06:40:18	6.5	24.8	A	0.5786
15	ESM	MZ19	Central Italy	30/10/2016	06:40:18	6.5	22.6	A	0.6419
16	ESM	ULA	Northwestern Balkan Peninsula	15/04/1979	06:19:41	6.9	19.7	A	0.5185
17	ESM	ATH4	Greece	07/09/1999	11:56:49	5.9	19.7	A	3.0668
18	ESM	CLO	Central Italy	26/10/2016	19:18:06	5.9	10.8	A	1.3670
19	ESM	MMO	Central Italy	26/10/2016	19:18:06	5.9	16.2	A	2.2189
20	ESM	MNF	Central Italy	26/10/2016	19:18:06	5.9	17.4	A	2.3110

Table A.14
Ground motion records selected for $T_R = 475$ years and used for the NTHAs of the SR-H building

n.	Database	Station ID	Earthquake Name	Date	Time (UTC)	Mw	Epicentral Distance (km)	Site class	Scale Factor
1	ESD	ST54	Tabas	16/09/1978	15:35:57	7.3	12	A	0.7630
2	ESD	ST225	Valnerina	19/09/1979	21:35:37	5.8	5	A	3.7958
3	ESD	ST96	Campano Lucano	23/11/1980	18:34:52	6.9	32	A	0.4491
4	ESD	ST561	Izmit	17/08/1999	00:01:40	7.6	47	A	1.2354
5	ESD	ST2486	South Iceland	17/06/2000	15:40:41	6.5	5	A	0.3692
6	ESD	ST2487	South Iceland	17/06/2000	15:40:41	6.5	13	A	1.8395
7	ESD	ST1320	Kozani	13/05/1995	08:47:15	6.5	17	A	4.0379
8	ESD	ST2496	South Iceland (aftershock)	21/06/2000	00:51:48	6.4	14	A	1.3101
9	ESD	ST2486	South Iceland (aftershock)	21/06/2000	00:51:48	6.4	22	A	3.2446
10	ESD	ST2557	South Iceland (aftershock)	21/06/2000	00:51:48	6.4	15	A	1.3602
11	ESD	ST2556	South Iceland (aftershock)	21/06/2000	00:51:48	6.4	20	A	1.8161
12	ESD	ST2558	South Iceland (aftershock)	21/06/2000	00:51:48	6.4	5	A	0.4598
13	ESD	ST539	Bingol	01/05/2003	00:27:04	6.3	14	A	0.8923
14	ESM	MZ19	Central Italy	30/10/2016	06:40:18	6.5	22.6	A	0.8798
15	ESM	ULA	Northwestern Balkan Peninsula	15/04/1979	06:19:41	6.9	19.7	A	0.7106
16	ESM	CLO	Central Italy	26/10/2016	19:18:06	5.9	10.8	A	1.8736
17	ESM	MMO	Central Italy	30/10/2016	06:40:18	6.5	19.2	A	2.9162
18	ESM	MNF	Central Italy	26/10/2016	19:18:06	5.9	17.4	A	3.1674
19	ESM	T1213	Central Italy	30/10/2016	06:40:18	6.5	12	A	0.6164
20	ESM	4101	Izmit	17/08/1999	00:01:38	7.6	3.4	A	0.6064

Table A.15
Ground motion records selected for TR = 975 years and used for the NTHAs of the SR-H building

n.	Database	Station ID	Earthquake Name	Date	Time (UTC)	Mw	Epicentral Distance (km)	Site class	Scale Factor
1	ESD	ST20	Friuli	06/05/1976	20:00:13	6.5	23	A	2.1550
2	ESD	ST96	Campano Lucano	23/11/1980	18:34:52	6.9	32	A	0.6138
3	ESD	ST98	Campano Lucano	23/11/1980	18:34:52	6.9	25	A	4.1769
4	ESD	ST561	Izmit	17/08/1999	00:01:40	7.6	47	A	1.6882
5	ESD	ST575	Izmit	17/08/1999	00:01:40	7.6	9	A	0.8574
6	ESD	ST2486	South Iceland	17/06/2000	15:40:41	6.5	5	A	0.5046
7	ESD	ST2552	South Iceland	17/06/2000	15:40:41	6.5	41	A	4.9498
8	ESD	ST2496	South Iceland (aftershock)	21/06/2000	00:51:48	6.4	14	A	1.7903
9	ESD	ST2486	South Iceland (aftershock)	21/06/2000	00:51:48	6.4	22	A	4.4338
10	ESD	ST2557	South Iceland (aftershock)	21/06/2000	00:51:48	6.4	15	A	1.8587
11	ESD	ST2563	South Iceland (aftershock)	21/06/2000	00:51:48	6.4	24	A	4.5090
12	ESD	ST2497	South Iceland (aftershock)	21/06/2000	00:51:48	6.4	20	A	2.7624
13	ESD	ST539	Bingol	01/05/2003	00:27:04	6.3	14	A	1.2194
14	ESM	MZ19	Central Italy	30/10/2016	06:40:18	6.5	22.6	A	1.2023
15	ESM	ULA	Northwestern Balkan Peninsula	15/04/1979	06:19:41	6.9	19.7	A	0.9711
16	ESM	CLO	Central Italy	26/10/2016	19:18:06	5.9	10.8	A	2.5603
17	ESM	CLO	Central Italy	30/10/2016	06:40:18	6.5	7.8	A	0.5250
18	ESM	MMO	Central Italy	26/10/2016	19:18:06	5.9	16.2	A	4.1558
19	ESM	MMO	Central Italy	30/10/2016	06:40:18	6.5	19.2	A	3.9851
20	ESM	T1213	Central Italy	30/10/2016	06:40:18	6.5	12	A	0.8423

References

[1] Fajfar P. Capacity spectrum method based on inelastic demand spectra. Earthq Eng Struct Dynam 1999;28:979–93. https://doi.org/10.1002/(SICI)1096-9845(199909)28:9<979::AID-EQE850>3.0.CO;2-1.

[2] Fajfar P. A nonlinear analysis method for performance-based seismic design. Earthq Spectra 2000;16(3):573–92. https://doi.org/10.1193/1.1586128.

[3] NTC2018 (D.M. 17/01/2018). Decreto del Ministero delle Infrastrutture e dei trasporti del 17/01/2018. Aggiornamento delle Norme Tecniche per le Costruzioni, *Gazzetta Ufficiale Serie generale n.* vol. 42 *del 20/02/2018*, Roma (in Italian).

[4] Eurocode 8 - Part 1: Eurocode 8. Design provisions for earthquake resistance of structures. Part 1-1: general rules – seismic actions and general requirements for structures. ENV 1998-1. Brussels: CEN; 2005.

[5] Gupta B, Kunnath SK. Adaptive spectra-based pushover procedure for seismic evaluation of structures. Earthq Spectra 2000;16(2):367–91. https://doi.org/10.1193/1.1586117.

[6] Antoniou S, Pinho R. Advantages and limitations of adaptive and non-adaptive force-based pushover procedures. J Earthq Eng 2004;8(4):497–522. https://doi.org/10.1080/13632460409350498.

[7] Chopra AK, Goel RK. A modal pushover procedure to estimate seismic demands of buildings. Earthq Eng Struct Dynam 2002;31:561–82. https://doi.org/10.1002/eqe.144.

[8] Fajfar P, Marusic D, Perus I. Torsional effects in the pushover-based seismic analysis of buildings. J Earthq Eng 2005;9:831–54. https://doi.org/10.1080/13632460509350568.

[9] Kreslin M, Fajfar P. The extended N2 method considering higher mode effects in both plan and elevation. Bull Earthq Eng 2012;10:695–715. https://doi.org/10.1007/s10518-011-9319-6.

[10] Bosco M, Ghersi A, Marino EM. Corrective eccentricities for assessment by the nonlinear static method of 3D structures subjected to bidirectional ground motions. Earthq Eng Struct Dynam 2012;41:1751–73. https://doi.org/10.1002/eqe.2155.

[11] Anagnostopoulos SA, Alexopoulou C, Stathopoulos KG. An answer to an important controversy and the need for caution when using simple models to predict inelastic earthquake response of buildings with torsion. Earthq Eng Struct Dynam 2010;39:521–40. https://doi.org/10.1002/eqe.957.

[12] Kosmopoulos AJ, Fardis MN. Estimation of inelastic seismic deformations in asymmetric multistorey RC buildings. Earthq Eng Struct Dynam 2007;36(9):1209–34. https://doi.org/10.1002/eqe.678.

[13] Belejo A, Bento R. Improved modal pushover analysis in seismic assessment of asymmetric plan buildings under the influence of one and two horizontal components of ground motions. Soil Dynam Earthq Eng 2016;87:1–15. https://doi.org/10.1016/j.soildyn.2016.04.011.

[14] Oyguc R, Toros C, Abdelnaby AE. Seismic behavior of irregular reinforced-concrete structures under multiple earthquake excitations. Soil Dynam Earthq Eng 2018;104:15–32. https://doi.org/10.1016/j.soildyn.2017.10.002.

[15] Erduran E. Assessment of current nonlinear static procedures on the estimation of torsional effects in low-rise frame buildings. Eng Struct 2008;30(9):2548–58. https://doi.org/10.1016/j.engstruct.2008.02.008.

[16] Bosco M, Ghersi A, Marino EM, Rossi PP. Comparison of nonlinear static methods for the assessment of asymmetric buildings. Bull Earthq Eng 2013;11(6):2287–308. https://doi.org/10.1007/s10518-013-9516-6.

[17] D'Ambrisi A, De Stefano M, Tanganelli M. Use of pushover analysis for predicting seismic response of irregular buildings: a case study. J Earthq Eng 2009;13(8):1089–100. https://doi.org/10.1080/13632460902898308.

[18] Bhatt C, Bento R. Assessing the seismic response of existing RC buildings using the extended N2 method. Bull Earthq Eng 2011;9(4):1183–201. https://doi.org/10.1007/s10518-011-9252-8.

[19] Cantagallo C, Camata G, Spacone E. A probability-based approach for the definition of the expected seismic damage evaluated with non-linear time-history analyses. J Earthq Eng 2019;23(2):261–83. https://doi.org/10.1080/13632469.2017.1323043.

[20] Giannopoulos D, Vamvatsikos D. Ground motion records for seismic performance assessment: to rotate or not to rotate? Earthq Eng Struct Dynam 2018;47(12):2410–25. https://doi.org/10.1002/eqe.3090.

[21] Skoulidou D, Romão X. The significance of considering multiple angles of seismic incidence for estimating engineering demand parameters. Bull Earthq Eng 2020;18(1):139–63. https://doi.org/10.1007/s10518-019-00724-y.

[22] Daei A, Poursha M. On the accuracy of enhanced pushover procedures for seismic performance evaluation of code-conforming RC moment-resisting frame buildings subjected to pulse-like and non-pulse-like excitations. Structures 2021;32:929–45. https://doi.org/10.1016/j.istruc.2021.03.035.

[23] Ministero dei lavori pubblici, Decreto ministeriale del 30/05/1974, Norme tecniche per la esecuzione delle opere in cemento armato normale e precompresso e per le strutture metalliche, *Gazzetta Ufficiale Serie generale n. 198 del 29/07/1974*, Roma (in Italian).

[24] Ministero dei lavori pubblici, Decreto ministeriale del 19/06/1984, Norme tecniche per le costruzioni in zone sismiche, *Gazzetta Ufficiale Serie generale n. 208 del 30/07/1984*, Roma (in Italian).

[25] Ministero dei lavori pubblici, Decreto ministeriale del 1/04/1983, Norme tecniche per la esecuzione delle opere in cemento armato normale e precompresso e per le strutture metalliche, *Gazzetta Ufficiale Serie generale n.* 224 *del 17/08/1983*, Roma (in Italian).

[26] Ministero dei lavori pubblici, Decreto ministeriale del 16/01/1996, Norme tecniche relative ai «Criteri generali per la verifica di sicurezza delle costruzioni e dei carichi e sovraccarichi», *Gazzetta Ufficiale Serie generale n.* 29 del 5/02/1996, Roma (in Italian).

[27] McKenna F, Scott MH, Fenves GL. Nonlinear finite-element analysis software architecture using object composition. J Comput Civ Eng 2010;24(1):95–107. https://doi.org/10.1061/(ASCE)CP.1943-5487.0000002.

[28] Petracca M, Candeloro F, Camata G. STKO user manual. Pescara: ASDEA Software Technology; 2017.

[29] Scott MH, Fenves GL. Plastic hinge integration methods for force-based beam-column elements. J Struct Eng 2006;132(2):244–52. https://doi.org/10.1061/(ASCE)0733-9445(2006)132:2(244).

[30] Spacone E, Filippou FC, Taucer FF. Fibre beam–column model for non-linear analysis of R/C frames: Part I. Formulation. Earthq Eng Struct Dynam 1996;25(7):711–25. https://doi.org/10.1002/(SICI)1096-9845(199607)25:7<711::AID-EQE576>3.0.CO;2-9.

[31] Aci 318-19: building code requirements for structural concrete and commentary. Farmington Hills, MI, USA: American Concrete Institute; 2019.

[32] Kent DC, Park R. Flexural members with confined concrete. J Struct Div 1971. https://doi.org/10.1061/JSDEAG.0002957. ASCE; 97:ST7.

[33] Mazzoni S, McKenna F, Scott MH, Fenves GL. OpenSees command language manual. Pacif Earthq Eng Res(PEER) Center 2006;264:137–58.

[34] Terrenzi M, Spacone E, Camata G. Comparison between phenomenological and fiber-section non-linear models. Front Built Environ 2020;6:38. https://doi.org/10.3389/fbuil.2020.00038.

[35] Haselton CB, Liel AB, Taylor Lange S, Deierlein GG. Beam-column element model calibrated for predicting flexural response leading to global collapse of rc frame buildings. Pacific Earthquake Engineering Research Center PEER; 2008.
[36] Ibarra LF, Medina RA, Krawinkler H. Hysteretic models that incorporate strength and stiffness deterioration. Eng Struct Dynam 2005;34:1489–511. https://doi.org/10.1002/eqe.495.
[37] Barbagallo F, Bosco M, Marino EM, Rossi PP. On the fibre modelling of beams in RC framed buildings with rigid diaphragm. Bull Earthq Eng 2020;18(1):189–210. https://doi.org/10.1007/s10518-019-00723-z.
[38] Hejal R, Chopra AK. Lateral-torsional coupling in earthquake response of frame buildings. ASCE J Struct Eng 1989;115(4):852–67. https://doi.org/10.1061/(ASCE)0733-9445(1989)115:4(852). 10.1061/(ASCE)0733-9445(1989)115:4(852).
[39] Fajfar P, Fischinger M. Non-linear seismic analysis of RC buildings: implications of a case study. Eur Earthq Eng 1987;1:31–43.
[40] Saiidi M, Sozen MA. Simple nonlinear seismic analysis of R/C structures. J Struct Div 1981;107(5):937–53. https://doi.org/10.1061/JSDEAG.0005714.
[41] Fajfar P, Gašperšič P. The N2 method for the seismic damage analysis of RC buildings. Earthq Eng Struct Dynam 1996;25(1):31–46. https://doi.org/10.1002/(SICI)1096-9845(199601)25:1<31::AID-EQE534>3.0.CO;2-V.
[42] Fajfar P, Gašperšič P, Drobnič D. A simplified nonlinear method for seismic damage analysis of structures. In: Fajfar P, Krawinkler H, editors. Seismic design methodologies for the next generation of codes. Rotterdam: Balkema; 1997. p. 183–94.
[43] Barbagallo F, Di Domenico M, Terrenzi M, Cantagallo C, Marino EM, Ricci P, Verderame GM, Camata C, Spacone E. Influence of the modelling approach on the seismic assessment of RC structures by nonlinear static analyses. Soil Dynam Earthq Eng 2023;172. https://doi.org/10.1016/j.soildyn.2023.107970.
[44] Fema356. Prestandard and commentary for the seismic rehabilitation of buildings. Washington: Federal Emergency Management Agency; 2000.
[45] ASCE/SEI 41-06. Seismic rehabilitation of existing building. American Society of Civil Engineers; 2007.
[46] ASCE/SEI 41-17. Seismic evaluation and retrofit of existing buildings. Reston, VA, USA: American Society of Civil Engineers; 2017.
[47] Fujii K. Assessment of pushover-based method to a building with bidirectional set-back. Earthq Struct 2016;11(3):421–43. https://doi.org/10.12989/eas.2016.11.3.421.
[48] Magliulo G, Maddaloni G, Cosenza E. Extension of N2 method to plan irregular buildings considering accidental eccentricity. Soil Dynam Earthq Eng 2012;43:69–84. https://doi.org/10.1016/j.soildyn.2012.07.032.
[49] Charney FA. Unintended consequences of modeling damping in structures. ASCE J Struct Eng 2008;134(4):581–92. https://doi.org/10.1061/(ASCE)0733-9445(2008)134:4(581).
[50] Ambraseys N, Smit P, Sigbjornsson R, Suhadolc P, Margaris B. Internet-site for European strong-motion data. European Commission, Research-Directorate General, Environment and Climate Programme; 2002.
[51] Luzi L, Puglia R, Russo E. ORFEUS WG5. Engineering strong motion database, version 1.0. Istituto Nazionale di Geofisica e Vulcanologia, Observatories & Research Facilities for European Seismology; 2016. https://doi.org/10.13127/ESM.
[52] Beyer K, Bommer JJ. Relationships between median values and between aleatory variabilities for different definitions of the horizontal component of motion. Bull Seismol Soc Am 2006;96(4A):1512–22. https://doi.org/10.1785/0120050210.
[53] Shome N, Cornell CA. Probabilistic seismic demand analysis of nonlinear structures. In: Report RMS-35, reliability of marine structures program. Stanford, CA: Stanford University; 1999.
[54] Cantagallo C, Camata G, Spacone E. Influence of ground motion selection methods on seismic directionality effects. Earthq Struct 2015;8(1):185–204. https://doi.org/10.12989/eas.2015.8.1.185.
[55] Bommer JJ, Acevedo AB. The use of real earthquake accelerograms as input to dynamic analysis. J Earthq Eng 2004;8(1):43–91. https://doi.org/10.1080/13632460409350521.
[56] Vanmarke EH. Representation of earthquake ground motion: scaled accelerograms and equivalent response spectra. State-of-the-Art for assessing earthquake hazards in the United States. Mississippi: U.S. Army Engineers Waterways Experiment Station, Vicksburg; 1979. Miscellaneous Paper S-73-1, Report 14.
[57] Krinitzsky EL, Chang FK. State-of-the-art for assessing earthquake hazards in the United States: specifying peak motions for design earthquakes. Vicksburg, Mississippi: U.S. Army Engineers Waterways Experiment Station; 1977. Miscellaneous Paper S-73-1, Report 7.
[58] Boore DM. Simulation of ground motion using the stochastic method. Pure Appl Geophys 2003;160:635–76. https://doi.org/10.1007/PL00012553.
[59] Gasparini DA, Vanmarcke EH. Simulated earthquake motions compatible with prescribed response spectra. In: Evaluation of seismic safety of buildings report No. 2. Cambridge, Massachusetts: Department of Civil Engineering, MIT; 1979.
[60] Cantagallo C, Camata G, Spacone E, Corotis R. The variability of deformation demand with ground motion intensity. Probabilist Eng Mech 2012;28:59–65. https://doi.org/10.1016/j.probengmech.2011.08.016.
[61] Cantagallo C, Camata G, Spacone. Seismic demand sensitivity of reinforced concrete structures to ground motion selection and modification methods. Earthq Spectra 2014;30(4):1449–65. https://doi.org/10.1193/062812EQS226M.
[62] Faggella M, Barbosa AR, Conte JP, Spacone E, Restrepo JI. Probabilistic seismic response analysis of a 3-D reinforced concrete building. Struct Saf 2013;44:11–27.